Inference for stochastic kinetic models from multiple data sources for joint estimation of infection dynamics from aggregate reports and virological data

Yury E. García[*], Oksana A. Chkrebtii[*], Marcos A. Capistrán, Daniel E. Noyola [†]

December 15, 2024

Abstract

Influenza and respiratory syncytial virus (RSV) are the leading etiological agents of seasonal acute respiratory infections (ARI) around the world. Medical doctors typically base the diagnosis of ARI on patients' symptoms alone, and do not always

[*]These authors contributed equally

[†]**Yury E. García is PhD Student in Applied Mathematics at Centro de Investigación en Matemáticas A.C., Jalisco S/N Col. Valenciana, CP: 36240, Guanajuato, Gto. México (E-mail: yury@cimat.mx)**. **Oksana A. Chkrebtii** is Assistant Professor at Department of Statistics, The Ohio State University, 1958 Neil Ave, Columbus, OH 43210 (E-mail: oksana@osu.edu). **Marcos Capistrán** is Professor of Mathematics at Centro de Investigación en Matemáticas A.C., Jalisco S/N Col. Valenciana, CP: 36240, Guanajuato, Gto. México (E-mail: marcos@cimat.mx). **Daniel E. Noyola** is Research Professor at Department of Microbiology, Faculty of Medicine, Universidad Autónoma de San Luis Potosí, Av. Venustiano Carranza 2405, CP 78210, San Luis Potosí, México (E-mail: dnoyola@uaslp.mx).
This research was supported in part by the Mathematical Biosciences Institute (MBI) and the National Science Foundation under grant DMS 1440386. The authors thank Grzegorz A. Rempala (MBI) and Leticia Ramirez (CIMAT) for helpful comments and suggestions. The authors also thank The Ohio State University and Centro de Investigación en Matemáticas (CIMAT).

conduct virological tests necessary to identify individual viruses, which limits the ability to study the interaction between multiple pathogens and make public health recommendations. We consider a stochastic kinetic model (SKM) for two interacting ARI pathogens circulating in a large population and an empirically motivated background process for infections with other pathogens causing similar symptoms. An extended marginal sampling approach based on the Linear Noise Approximation to the SKM integrates multiple data sources and additional model components. We infer the parameters defining the pathogens' dynamics and interaction within a Bayesian hierarchical model and explore the posterior trajectories of infections for each illness based on aggregate infection reports from six epidemic seasons collected by the state health department, and a subset of virological tests from a sentinel program at a general hospital in San Luis Potosí, México. We interpret the results based on real and simulated data and make recommendations for future data collection strategies. Supplementary materials and software are provided online.

Keywords: Acute respiratory disease, Bayesian hierarchical modeling, Linear noise approximation, Influenza, Respiratory syncytial virus

1 INTRODUCTION

Inference on mathematical models of epidemic dynamics has become a powerful tool in the prediction, assessment, and control of disease outbreaks (Star and Moghadas 2010; Huppert and Katriel 2013; Siettos and Russo 2013). Such models are predominantly stochastic, reflecting the random nature of a large number of human interactions which enable infections to spread and individuals to change their infection status. The probabilities

of discrete transitions from one infection state to another are defined up to a set of unknown parameters, which may be inferred from observed data. The most widely used models are variations on the "Susceptible-(Exposed-)Infected-Recovered" (SIR/SEIR) formulation, which describes the temporal evolution of the proportion of individuals in each infection state at a given time. A variety of strategies have been developed to incorporate process-specific demographic stochasticity in this compartmental model. For example, Dukic et al. (2012) model process stochasticity by an additive white noise process on the growth rate of the infectious population computed from states that evolve according to the deterministic compartmental dynamics described above. In a different approach, Farah et al. (2014) assume additive process noise on the infection states of a deterministic SEIR model. Another approach is taken by Shrestha et al. (2011) by modeling infection state counts as multinomial processes with probabilities of inclusion obtained by first solving the ODE corresponding to the compartmental model and then solving for the transition probabilities as functions of current states. Another popular class of models, considered in this paper, describes process noise by modeling each individual interaction directly. This approach is based on stochastic kinetic modeling (e.g., Wilkinson (2006)), a first-principles interpretation of SIR dynamics inspired by chemical mass-action kinetics where molecules interact and change state according to specified transition probabilities. This approach accurately reflects inherent stochasticity in infection states because it naturally models individual-level transitions from one infection state to another as stochastic processes incorporating assumptions about both the disease and the interactions. However, estimation for such models poses a unique set of challenges. For a small population or one where state transitions can

be observed directly, posterior inference on the SKM parameters can exploit closed form expressions for full conditional distributions (Boys et al. 2008; Choi and Rempala 2011), but even for moderately sized populations, individual interactions and transitions become increasingly difficult to simulate and marginalize over. Furthermore, since data typically consists of observed infection counts rather than individual transition times, computation of the likelihood becomes computationally infeasible. To resolve this issue, a common strategy is to construct the likelihood based on a large-volume limit via diffusion approximation of the SKM (Van Kampen 1992), also known as the Linear Noise Approximation (LNA). Inference for model parameters based on this approximation was conducted in work by Komorowski et al. (2009); Golightly and Wilkinson (2011); Fearnhead et al. (2014); Golightly et al. (2015). However, challenges still remain in applying this approach to realistic data scenarios, such as conditioning on multiple data types that depend on the unknown infection states, and introducing model components to describe unmodeled disease states or account for model discrepancy. The contribution of the present work is to address these challenges by generalizing the approach of Fearnhead et al. (2014), which allows us to address the motivating problem of inference on the dynamics of two interacting pathogens from both aggregated infection reports and a subset of virological data collected in the state of San Luis Potosí, México. The ability to utilize multiple data sources allows estimation of parameters involved in the interaction of different pathogens that cause similar symptoms. Indeed, to our knowledge, our approach is the first to directly recover cross-interference parameters in a SKM for two pathogens as part of an overall hierarchical Bayesian inferential framework. We additionally identify and address practical challenges

of working with such models, including posterior sampling strategies that are well suited to such situations.

The article is organized as follows. The motivating application and the data are described in detail in Section 2. Section 3 begins by constructing a SKM for the evolution of individual infection states of the acute respiratory pathogens influenza and RSV and then describes its limiting behaviour in the large-population limit. A Bayesian hierarchical model is then formulated relating aggregated infection counts and a subset of virological tests to the SKM for infection states of the two pathogens augmented by a background model component representing infection by other pathogens. The inferential strategy is described in Section 4. Section 5 describes the results of the analysis based on six years of real and simulated data and provides a discussion of identifiability in the context of the multi-pathogen problem, using simulation to shed light on model identification under two data availability scenarios. Finally, Section 6 discusses the feasibility of our approach, summarizes our findings, and offers some perspectives on future work. Software to reproduce all results is provided at `github.com/ochkrebtii/Multipathogen-ARI-dynamics` (upon publication).

2 MOTIVATING APPLICATION

ARI are infections of the upper and lower respiratory tract caused by multiple etiological agents, most frequently, adenovirus, influenza A and B, parainfluenza, RSV, and rhinovirus. An important public health concern around the world, ARIs are responsible for substantial

mortality and morbidity (Thompson et al. 2003; Troeger et al. 2018), mainly affecting children under 5 and adults over 65 years of age (Kuri-Morales et al. 2006). Understanding of the underlying mechanisms of spread, transmission, and, importantly, cross-interference between these pathogens aids policy makers in assessing public health strategies and decision-making (Huppert and Katriel 2013).

Although different viruses are responsible for ARI, a substantial part of the burden of ARI in most regions is due to influenza and RSV (Chan et al. 2014; Velasco-Hernández et al. 2015; Chaw et al. 2016). The interaction and temporal dynamics of these pathogens are complex. Evidence suggests that influenza and RSV are seasonally related (Mangtani et al. 2006; Bloom-Feshbach et al. 2013) and circulate at similar times of the year in some temperate zones (Bloom-Feshbach et al. 2013; Velasco-Hernández et al. 2015). Because of their interaction and interference, these infections do not usually reach their epidemic peaks simultaneously (Ånestad 1987; Anestad et al. 1982; Anestad and Nordbo 2009), with peak times typically differing by less than one month (Bloom-Feshbach et al. 2013). In the clinical setting, it is difficult to determine which pathogen may be responsible for a patient's ARI, because of their overlapping circulation times and similar symptoms. Furthermore, laboratory tests necessary for identification of the virus are not conducted in most patients (Chan et al. 2014).

Our analysis is based on data from epidemic seasons 2003-2004 through 2008-2009, beginning in the first week of August and ending in the last week of July of the following year. Specifically, we use data on weekly aggregated morbidity reports and virological time series obtained in the state of San Luis Potosí, México. Morbidity reports consist of weekly

reports of ARI that required medical attention[1] at all community clinics and hospitals in the state that were reported to the State Health Service Epidemiology Department. The virological data was obtained from records of the Virology Laboratory (Facultad de Medicina, UASLP, San Luis Potosí, México) and consists of weekly counts of positive tests for RSV and influenza as well as tests which were negative for both pathogens. These virological tests were performed on all eligible pediatric patients (children under 5 years of age) admitted with lower respiratory infections (Gómez-Villa et al. 2017; Vizcarra-Ugalde et al. 2016) to Hospital Central "Dr. Ignacio Morones Prieto". Available data indicate that when these viruses present in community outbreaks, they tend to affect all age groups at the same time. Although the precise time of influenza epidemic onset and peak may vary slightly between age groups, influenza outbreaks tend to be synchronized across age groups (Wu et al. 2016). In addition, influenza surveillance data, such as that reported from Australia in 2017, shows similar influenza epidemic curves across different age groups (Australian Government Department of Health 2017). Detailed transmission studies show that RSV cases frequently present around the same time in different age groups within a household (Munywoki et al. 2013). Additionally, these virological tests are unlikely to reflect only small-scale outbreaks, since Hospital Central "Dr. Ignacio Morones Prieto" admits patients from all regions of the state. Though the number of virological tests is small relative to the total number of aggregated ARI reports, the systematic sampling of patients year-round, irrespective of the identification of an epidemic by any given virus, provides information on the period of circulation of influenza and RSV.

[1]This category includes all cases corresponding to the International Classification of Disease, 10th review (ICD-10) codes: J00-J06, J20, J21, except J02.0 and J03.0

3 MODELING

This section describes a SKM of influenza and RSV dynamics, as well as its diffusion approximation in the large-population limit, required to compute the likelihood of reported infection data and virological tests. We then construct a Bayesian hierarchical model that relates the governing equations, including a background infection component, to the aggregated ARI reports and the virological tests.

3.1 Stochastic Kinetic Model of a two-Pathogen System

Stochasticity is inherent in biological systems due to their discrete nature and the occurrence of environmental and demographic events. In the case of disease dynamics, the occurrence of events such as interactions between individuals that constitute exposure can be reasonably described as stochastic. Therefore it is reasonable to model this stochasticity directly in the individual transitions, in contrast to indirectly modeling their aggregate behavior or perturbing a deterministic compartmental model. Stochastic Kinetic or Chemical Master Equation modeling (Allen 2008; Wilkinson 2011) is a mathematical formulation of Markovian stochastic processes which describe the evolution of the probability distribution of finding the system in a given state at a specified time (Gillespie 2007; Thomas et al. 2012).

To model the relationship between influenza and RSV (henceforward called pathogens 1 and 2 respectively) during a single year, we consider a closed population of size Ω, assumed to be well mixed and homogeneously distributed, where the individuals interacting in a fixed region can make any of $\mathcal{R}$ possible transitions. The stochastic "Susceptible-Infected-Recovered"

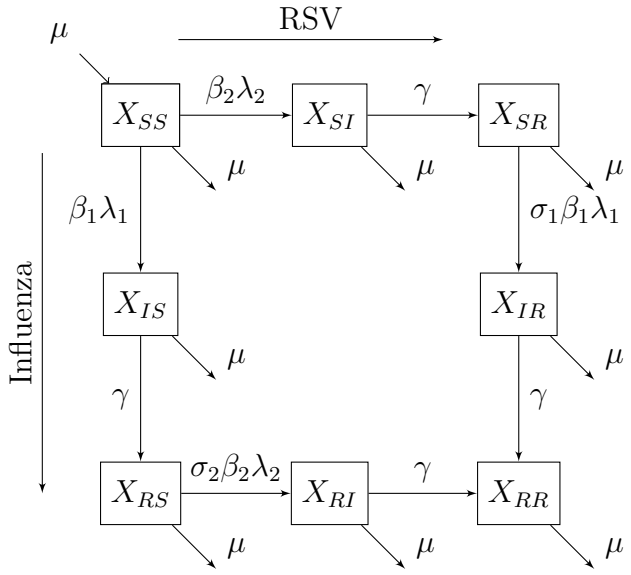

Figure 1: SIR model with two pathogens. X_{kl} represents the number of individuals in immunological status k for pathogen 1 and status l for pathogen 2. Labels above the arrows represent the reaction rates for each reaction type.

(SIR) model with two pathogens (Kamo and Sasaki 2002; Adams and Boots 2007; Vasco et al. 2007) is described by eight compartments corresponding to distinct immunological statuses. Denote by $X_{kl}(t)$ the *number of individuals* at time t in immunological status $k \in \{S, I, R\}$ for pathogen 1 and immunological status $l \in \{S, I, R\}$ for pathogen 2. We omit the state X_{II} from the model because, although simultaneous infection by both viruses is biologically possible, clinical studies have found that the frequency of co-infection with RSV and influenza is usually low (Meskill et al. 2017).

In our model, the constants β_1 and β_2 represent the contact transmission rate, which describes the flow of individuals from the susceptible group to a group infected with pathogen 1 and 2 respectively. In the context of ARI, the average recovery time is known

to be relatively stable and lasts for approximately 7 days (Centers for Disease Control and Prevention 2008). Therefore, the rate, γ, at which infected individuals recover (move from infected to temporary immunity in the recovered category) is $1/7\ days^{-1}$. Since the population is relatively stable over the years under study, we set the birth rate equal to the death rate μ in our transition model. We also assume an average life expectancy of $1/\mu = 70\ years^{-1}$ (World Health Organization 2017). Variables λ_1 and λ_2 represent the proportion of the population infected with pathogens 1 and 2 respectively at a given time. Finally, to describe the interaction between influenza and RSV, we use the cross-immunity or cross-enhancement parameters σ_1 and σ_2. Cross-immunity for influenza is present when $0 < \sigma_1 < 1$, indicating that the presence of RSV inhibits infection with influenza. A value of $\sigma_1 = 0$ confers complete protection against influenza while a value of $\sigma_1 = 1$ confers no protection; and a value of $\sigma_1 > 1$ represents increasing degree of cross-enhancement, indicating that the presence of RSV enhances the presence influenza (Adams and Boots 2007). The definition of σ_2 is analogous. Further customization of the transition mechanism is possible within this stochastic dynamical model (e.g. Wilkinson 2006), and is desirable when additional information about the system dynamics is available. Examples include considering the effect of vaccination programs, seasonal forcing, or the presence of specific additional pathogens in circulation. We discuss these in the section on future work.

We next make the following standard assumptions on the infection states X. Transitions from one state to another depend only on the time interval but not on absolute time, mathematically, $X(\Delta t) - X(0)$ and $X(t+\Delta t) - X(t)$ are identically distributed. Additionally, the probability of two or more transitions occurring simultaneously is assumed to be zero.

Table 1: Parameters defining the two-pathogen SKM for influenza and RSV

Parameter	**Description**
σ_1	Cross-immunity or enhancement for pathogen 1
σ_2	Cross-immunity or enhancement for pathogen 2
λ_p	Proportion of individuals infected with pathogen $p = 1, 2$
β_p	Baseline transmission rate for pathogen $p = 1, 2$
μ	Birth and death rate
γ	Recovery rate
Ω	Average yearly population size (assumed stable over time)

Since the model preserves mass, the constraint $\Omega = X_{SS} + X_{IS} + X_{SR} + X_{RS} + X_{SI} + X_{RR} + X_{RI} + X_{IR}$ is satisfied. The probability mass function p_t describing the probability of being in state $X = x$ at time t evolves according to the Kolmogorov forward equation (chemical master equation, or CME),

$$\frac{dp_t(x)}{dt} = \sum_{j=1}^{\mathcal{R}} \left\{ a_j(x - v_j) p_t(x - v_j) - a_j(x) p_t(x) \right\}, \tag{1}$$

where the transition probabilities $a_j(x)$ are obtained by multiplying the rates shown in Figure 1 by Δt sufficiently small (Gillespie 2007; Allen 2008), and $v_j(t)$ are stoichiometric vectors whose elements in $\{-1, 0, 1\}$ describe the addition or subtraction of mass from a particular compartment. A list with the $\mathcal{R}$ reactions and the explicit form of these terms are defined in the Supplement. The large-volume approximation to this system characterizes the distribution of the Markov process $X(t), t \in [0, T]$ as,

$$X(t) \mid \theta \sim \mathcal{N}\left(\Omega\phi(t) + \Omega^{1/2}\tilde{\xi}(t), \Omega C(t, t) \right), \; t \in [0, T]. \tag{2}$$

The next section defines the quantities $\phi, \tilde{\xi}, C$, and explains the above large-volume approximation.

Readers who are familiar with the details of the approximation may skip this section. Section 3.3 describes how this approximation is used to model aggregated report data.

3.2 Model Components via Linear Noise Approximation

A large-volume approximation of the CME (1) is given by the van Kampen expansion, which can then be computed via the Linear Noise Approximation (LNA) (Van Kampen 1992). For large Ω the system states X can be expressed as the sum of a deterministic term $\phi : [0, T] \to \mathbb{R}^{+\mathcal{S}}$ and a stochastic term ξ,

$$X(t) = \Omega\phi(t) + \Omega^{1/2}\xi(t), \quad t \in [0, T]. \tag{3}$$

Assuming constant average concentration, the size of the stochastic component will increase as the square root of population size. Let $S = [v_1, \ldots, v_{\mathcal{R}}]$ be a $\dim\{X(t)\}\times\mathcal{R}$ stoichiometric matrix that describes changes in the population size due to each of the $\mathcal{R}$ reactions. The time-evolution of the term of order $\Omega^{1/2}$ (Van Kampen 1992), $\phi_i(t) = \lim_{\Omega,X\longrightarrow\infty} X_i(t)/\Omega$ is governed by the ODE initial value problem,

$$\begin{cases} \dfrac{d\phi_i(t)}{dt} = \displaystyle\sum_{j=1}^{\mathcal{R}} S_{ij} a_j(\phi(t)), \quad t \in (0, T],\ i = 1, \ldots, \dim\{X(t)\}, \\ \phi_i(0) = \phi_0, \qquad\qquad\qquad\qquad\qquad\qquad i = 1, \ldots, \dim\{X(t)\}. \end{cases} \tag{4}$$

where $\phi_0 = X(0)/\Omega$. The stochastic process ξ is governed by the Itô diffusion equation,

$$d\xi(t) = A(t)\xi(t)dt + \sqrt{B(t)}dW(t), \quad t \in [0, T], \tag{5}$$

where $A(t) = \dfrac{\partial S\, a(\phi(t))}{\partial \phi(t)}$, $B(t) = S\,\mathrm{diag}\{a(\phi(t))\}\, S^{\top}$, and $W(t)$ denotes the $\mathcal{R}$ dimensional Wiener process (Van Kampen 1992; Gillespie 2007). For fixed or Gaussian initial conditions, the SDE in (5) can be solved analytically. The solution of this equation is a Gaussian process with mean $\tilde{\xi}$ and covariance C (Van Kampen 1992), that is,

$$\xi(t) \sim \mathcal{N}\left(\tilde{\xi}\,(t)\,, C(t,t)\right), \quad t \in [0, T], \tag{6}$$

where $\tilde{\xi}(t)$ and $C(t,t)$ are obtained (see Van Kampen (1992), pp. 210-214) by solving the ODE initial value problem,

$$\begin{cases} \dfrac{\partial \tilde{\xi}(t)}{\partial t} = \Phi(t)\tilde{\xi}(0), \quad t \in (0, T], \\ \xi(0) = \tilde{\xi}_0, \end{cases} \tag{7}$$

where $\Phi(t)$ is the evolution, or fundamental matrix (Grimshaw 1991) determined by the matrix equation,

$$\begin{cases} \dot{\Phi}(t) = A(t)\Phi(t), \quad t \in (0, T], \\ \Phi(0) = I. \end{cases} \tag{8}$$

The covariance C is obtained by solving,

$$\begin{cases} \dfrac{dC(t)}{dt} = C(t)A(t)^T + A(t)C(t) + B(t), \quad t \in (0, T], \\ C(0) = C_0. \end{cases} \tag{9}$$

It follows from (3) and (6) that the transition densities of $X(t)$ are given by (2).

3.3 Probability Models for Aggregate Reports and Virological Tests

Our first data set consists of indirect observations of the Markov process $X(t) : t \in [0, T]$ transformed via $G^T = [0, 1, 0, 1, 1, 0, 1, 0]$. That is, observations are made on the total number $G^\top X = X_{IS}(t) + X_{IR}(t) + X_{SI}(t) + X_{RI}(t)$ of reported infections from influenza and RSV. Setting $\tilde{\xi}(0) = 0$, it follows that $\tilde{\xi}(t) = 0$ for all $t \in [0, T]$. Thus,

$$G^\top X(t_i) \mid \theta \sim \mathcal{N}\left(\Omega G^\top \phi(t_i),\, \Omega G^\top C(t_i) G\right),\ i = 1, \ldots, M, \tag{10}$$

where θ is a vector of the SKM parameters defined in Section 3.1, augmented with unknown initial conditions for X and prior variance on the state, $C_0 = c_0 \mathbb{I}_{\dim(X),\dim(X)}$,

$$\theta = [\beta_1, \beta_2, \sigma_1, \sigma_2, X(0), C_0]. \tag{11}$$

The aggregate number of ARI cases in the San Luis Potosí data also includes infections by viruses other than influenza and RSV. Although these may be responsible for a significant

fraction of all ARI cases, influenza and RSV are the two viruses that drive the epidemic fluctuations observed during the winter outbreaks in each year. Other viruses in circulation are included in the model by augmenting the state vector X by a background term corresponding to ARI infection that is not caused by Influenza or RSV. In contrast to infection states by Influenza or RSV, this background term is modelled empirically rather than mechanistically. It is reasonable to assume that the number of background infections during a given week is related to the previous week's up to process noise. This implies the autoregressive model,

$$D(t_i) = \Omega c + \nu D(t_{i-1}) + \eta(t_i),\ i = 1, \ldots, M, \tag{12}$$

where $|\nu| < 1$ and $\eta(t_i) \sim \mathcal{N}\left(0, \Omega^{3/2}\kappa\right), i = 1, \ldots, M$ are independent, zero-mean, stochastic terms. The order of the process noise was chosen to be between that of X (proportional to Ω) and of the observation error (proportional to Ω^2). This choice results in a background process that is more variable than the state X but is not flexible enough to over-fit the data. Moreover, to ensure comparable spread, we set $\kappa = c_0$, the prior process variance for the infection states X. As with any model discrepancy term, the integration of additional data or information (in our case, the results of virological tests) will help to constrain the background model (Brynjarsdóttir and O'Hagan 2014).

Observed aggregate counts are assumed subject to independent Normal observation errors with mean zero and variance $\Omega^2\Sigma$. We make the additional assumption that a fixed proportion, $r \in [0, 1]$, of all individuals infected with ARI seek consultation. Therefore, the

likelihood of the observed aggregated reports is,

$$
\begin{aligned}
&Y(t_i) \mid \phi(t_i), C(t_i), \theta, \tau \\
&\sim \mathcal{N}\left(r\Omega G^{\top}\phi(t_i) + r\Omega c/(1-\nu),\, r^2\Omega G^T C(t_i) G + r^2\Omega^{3/2}\kappa/(1-\nu^2) + \Omega^2\Sigma\right),\ i = 1, \ldots, M,
\end{aligned}
\tag{13}
$$

where τ is a vector containing auxiliary parameters not directly related to the SKM defined in Section 3.1,

$$\tau = [c, \nu, r, \Sigma].$$

The justification for modeling the total number of influenza and RSV infections directly via the Normal model obtained via the LNA is computational (Fearnhead et al. 2014; Golightly et al. 2015), by exploiting the availability of closed-form Bayesian updates over the states. Modeling counts via a discrete distribution centered at the LNA would require an additional layer of sampling at each observation location for each Markov chain Monte Carlo (MCMC) iteration, which would quickly become computationally infeasible.

Simulation results in Section 5.3 suggest that using aggregate counts (13) alone leaves some uncertainty about the circulation patterns of individual pathogen infection trajectories, and that the inclusion of the virological data described in Section 2 can aid in disaggregating the dynamics of the two pathogens. Denote by $N_1(t_i)$, $N_2(t_i)$, $N_3(t_i)$ the number of virological laboratory tests that identified influenza, RSV, and neither pathogen, respectively, for children under 5 years of age admitted with an ARI during week i at Hospital Central.

The total number of virological tests is related to the number of infected individuals in the population as follows. According to the 2010 census, there were $\Omega_c = 266,761$ children under 5 years of age in San Luis Potosí out of a total population of $\Omega = 2,585,518$ (Consejo Nacional de Población, México). Furthermore, available data suggests that approximately $r_h = 0.0005$ of children with reported ARI in the state are admitted to Hospital Central, and are therefore eligible for a virological test. Thus, we model the expected number of virological tests that were positive for influenza, RSV, and other background infections, respectively as,

$$
\begin{aligned}
m_{N_1}(t_i) &= \mathrm{E}\left(N_1(t_i) \mid X(t_i), \theta, \tau\right) = r_h r(\Omega_c/\Omega)\left(X_{IS}(t_i) + X_{IR}(t_i)\right),\ i = 1, \ldots, M, \\
m_{N_2}(t_i) &= \mathrm{E}\left(N_2(t_i) \mid X(t_i), \theta, \tau\right) = r_h r(\Omega_c/\Omega)\left(X_{SI}(t_i) + X_{RI}(t_i)\right),\ i = 1, \ldots, M, \\
m_{N_3}(t_i) &= \mathrm{E}\left(N_3(t_i) \mid X(t_i), D(t_i), \theta, \tau\right) = r_h r(\Omega_c/\Omega) D(t_i),\ i = 1, \ldots, M.
\end{aligned}
$$

The variability in the true proportion of the infected population admitted to Hospital Central, motivate the use of the variance-inflated model,

$$
N_k(t_i) \mid X(t_i), D(t_i)\theta, \tau \ \sim\ \mathrm{NegBin}\left(v\, m_{N_k}(t_i), 1/(1 + v^{-1})\right),\ k = 1, 2, 3,\ i = 1, \ldots, T, \tag{14}
$$

where v is an unknown variance inflation parameter. The variance of (14) is $m_k(t_i)\,(1 + 1/v)$ and is controlled by the unknown parameter v, which will be estimated along with the other model components.

Table 2: Parameters defining the observation and background models

Parameter	Description
c	AR-1 model additive constant term for the number of background infections
ν	AR-1 model coefficient for the number of background infections
v	Variance inflation factor for virological data
Σ	Observation noise variance
r	Reporting proportion for those infected with an ARI
r_h	Average proportion of total children with ARI admitted to the Hospital Central
Ω_c	Average yearly number of children under 5 years of age in San Luis Potosí

3.4 Prior Probability Model for Unknown Parameters

Prior distributions on the model and auxiliary parameters are obtained by expert elicitation and by enforcing physical constraints. For example, ensuring that initial conditions on the states represent the entire population requires that elements of the unknown initial state vector $X(0)/\Omega$ lie on the simplex, suggesting the use of a Dirichlet prior. Parameters that are constrained between 0 and 1, such as the reporting proportion r and the AR-1 coefficient ν for the background term, are assigned uniform prior distributions on $(0, 1)$. The remaining parameters are bounded below by zero, and are therefore assigned Gamma priors. The shape and scale hyperparameters for the Gamma prior on the transmission rates $\beta_p, p = 1, 2$, are chosen to be 20 and 3, respectively to yield a reasonable prior mean of 60 $days^{-1}$ and a large spread reflecting our uncertainty about these quantities. The shape and scale for the Gamma prior on the cross-interference parameters $\sigma_p, p = 1, 2$, are chosen to be 10 and 0.1, respectively. This choice places a relatively large prior weight on the region around the neutral case $\sigma_p = 1, p = 1, 2$. The same hyperparameters are chosen for the variance inflation factor, so that the prior mean corresponds to a relatively small spread in the counts of virological test data. The hyperprior on the prior variance c_0 of the

states and the prior on the error variance Σ are both Gamma with shape parameter 1 and scale parameter 0.01, ensuring moderately sized prior means on the scale of the population and substantial posterior mass near zero.

4 INFERENTIAL METHODOLOGY

4.1 Extended Marginal Sampling Approach based on LNA

In order to avoid expensive particle MCMC at each iteration of the sampling algorithm over the model parameters, Fearnhead et al. (2014) developed an approximate marginal approach based on Bayesian updating conditional on the partially observed state contaminated with Normal error. Instead of sampling from $p(x \mid \theta)$ for each proposed value of θ using, for example, an expensive Gillespie algorithm (Gillespie 2007), an approximate marginal likelihood $p_a(y \mid \theta)$ based on the LNA is obtained sequentially in closed form. This approach results from the repeated application of forecasting and analysis steps under a Kalman filtering framework (see Wikle and Berliner (2007) for a detailed discussion). The approximation comes from the fact that the operator that takes the state from time t_{i-1} to time t_i is nonlinear for SKMs. Nevertheless, simulations by Fearnhead et al. (2014) show that the method appears to correctly capture the model dynamics, while substantially reducing computational cost relative to direct inference. For this reason, this and related approximate techniques are the state of the art in the large population setting for fitting SKMs, as exact inference is typically computationally infeasible. For our analysis, this approach must be extended to integrate multiple data sources as well as including an

additional model discrepancy term. The argument that allows computation of $p_a(y \mid \theta)$ in closed form requires Normality and so cannot be applied directly to the virological data N.

Algorithm 1 in the Appendix summarizes the extended procedure. Due to the sequential nature of the algorithm, we use the subscript notation to denote time. For example $x_{1:i}$ denotes the vector of observed infection states x at times t_1 through t_i. We wish to sample from the posterior distribution over the unknown parameters and infection states. This is proportional to the prior multiplied by the likelihood components (2), (12), (14), and the approximate marginal likelihood $p_a\left(y_{1:M} \mid \theta, \tau\right)$,

$$\begin{aligned} & \pi_a\left(\theta, \tau, x_{1:M}, d_{1:M} \mid y_{1:M}, n_{1:M}\right) \\ \propto \; & p\left(n_{1:M} \mid x_{1:M}, d_{1:M}, y_{1:M}, \theta, \tau\right) \, p\left(x_{1:M}, d_{1:M} \mid y_{1:M}, \theta, \tau\right) \, p_a\left(y_{1:M} \mid \theta, \tau\right) \, \pi\left(\theta, \tau\right), \end{aligned} \tag{15}$$

assuming conditional independence between Y and N given the infection states, background, and parameters. The sequential application of forecast and analysis steps to obtain $p_a\left(y_{1:M} \mid \theta, \tau\right)$, provides the necessary information to sample from the approximate smoothing distribution over $x_{1:M}$ and $d_{1:M}$. This forms a likelihood-free step, conditional on which we can evaluate the likelihood component $p\left(n_{1:M} \mid x_{1:M}, d_{1:M}, y_{1:M}, \theta, \tau\right)$. This approach has the additional advantage of allowing us to visualize the posterior samples over the infection states and background, as well as to conduct one-step-ahead validation of the model by visualizing the posterior predictive distribution at each step.

4.2 Analysis of Multiple Years

The model formulated in Section 3 and the extended marginal sampling approach presented in Section 4.1 can, in principle, be applied over time domains of any length. However, in the context of our motivating problem, estimating the model for each epidemic year separately is consistent with the understanding of the way that different strains of influenza and RSV circulate from year to year. Parameters defining the circulation and interaction dynamics of influenza and RSV differ from strain to strain of the virus, and different strains of each virus circulate in different years. Specifically, RSV is classified into two major groups, A and B, each of which contains multiple variants (Venter et al. 2001; Mufson et al. 1988; Anderson et al. 1985). Of the five years studied by Peret et al. (1998), each year saw a shift in the predominant genotype or subtype of RSV, so that no single genotype or subtype was dominant for more than one of the five years. Peret et al. (1998) hypothesized that newly introduced strains are better able to evade previously induced immunity in the population and consequently either circulate more efficiently or are more pathogenic. Similarly, influenza viruses continually change due to antigenic drift, which requires vaccine reformulation before each annual epidemic (Ferguson et al. 2003), and antigenic shift (Centers for Disease Control and Prevention 2008; Zambon et al. 2001; Rambaut et al. 2008), which can lead to the emergence of new influenza epidemics. All of these effects combine to create unique conditions in each epidemic year. We note that sometimes such changes can occur within a single epidemic year, such as with the emergence of the global influenza A (H1N1) pandemic in April 2009. As will be seen in the analysis, the model fitted using data from the epidemic year 2008-2009 is only partially able to

capture the dynamics of this second epidemic wave of influenza in the latter part of the year.

5 RESULTS

This section describes the results of our analysis on both real and simulated data from San Luis Potosí.

5.1 Computational implementation

Posterior sampling was conducted by embedding the extended marginal sampling algorithm 1 for the states within a parallel tempering Markov chain Monte Carlo sampler (PTMCMC, Geyer 1991) over the unknown parameters. PTMCMC is suited to this application because it can effectively explore challenging posterior densities, with features such as ripples and ridges, which occurs when different combinations of parameters lead to similar model fits. 200,000 iterations of PTMCMC were obtained for each year using 8 parallel chains each. Due to strong posterior correlations between groups of parameters in our model, the parameters were sampled in three distinct blocks. One block consisted of the model parameters $\beta_1, \beta_2, \sigma_1, \sigma_2$. Another block consisted of prior state variance c_0 and parameters defining the observation processes, Σ, r, c, v, ν. Proposal covariance adaptation was performed for both blocks during the first 100,000 iterations, which were then discarded as burn-in. The last block consisted of the initial states X_{SS}, X_{IS}, X_{RS}, X_{SI}, X_{RI}, X_{SR}, X_{IR}, X_{RR}. For this block, only the proposal variances were adapted, because both the sign and

magnitude of posterior correlations between these quantities vary across the parameter space. Convergence was diagnosed by visual inspection of trace plots and correlation plots.

5.2 Inference Based on Data From San Luis Potosí, México

We examine the results for the motivating application of inferring the dynamics of influenza and RSV from aggregate ARI counts and auxiliary virological testing data from San Luis Potosí, México. Summaries of the marginal posterior distribution over ARI reports in the state are shown in Figures 2 and 3. Figure 3 illustrates marginal posterior summaries over disaggregated infection states (influenza, RSV, and background), while Figure 2 aggregates these summaries to allow for visual comparison with the data. Parameter estimates and credible intervals are provided in the Appendix.

In all the years examined except 2005-06, a single pathogen, either influenza or RSV, peaks first, followed by a peak associated with the other pathogen. Regardless of which peaks first, in all six years, the posterior trajectories agree with the patterns suggested by the virological test data. Specifically, in all years except 2003-04 and 2005-06, RSV cases peaks first, followed by influenza, with infections subsiding by the end of the epidemic year. In 2005-06, it appears that the first peak in aggregate infections may be due both influenza and RSV peaking at similar times, which is also consistent with the virological test data for that year. A secondary outbreak of RSV occurs later during that year and may be an indication of a new outbreak caused by a different strain of the virus than was circulating in the first half of the year. Secondary peaks that sometimes appear in the number of infections by a given pathogen may be due to the outbreak caused by a

different strain of that pathogen. Another possible explanation is geographical, with a new outbreak occurring in a different region that had not previously been exposed to the particular strain. The flexibility of our model to capture multiple epidemic peaks is useful, and will be further considered in light of recent literature in the Discussion.

For the most part, estimates of cross-interference parameters suggest that some degree of cross-enhancement exists between influenza and RSV, meaning that infection with one pathogen may be enhancing the chance of infection with the other. However, infection with the strains of RSV circulating in 2003-04 may have offered some protection against influenza, while the reverse appears to have occurred in 2008-09. Less strong evidence for such cross-immunity occurs for both pathogens in 2004-05, and for RSV in 2005-06, 2006-07, and 2008-09, based on the coverage of the credible intervals over the cross-interference parameters. The importance of enabling the estimation of cross-immunities, and consequently disaggregating pathogen dynamics, is highlighted in the Discussion section. Our analysis lends force to the argument that novel sentinel programs, like the one implemented at Hospital Central, provide a powerful tool to study these epidemics.

In order to obtain more insight into our analysis, a simulation was conducted as follows. For each year, the model parameters estimated from the real data were used to generate a synthetic data set. First, the Gillespie algorithm (Gillespie 2007) was used to simulate a trajectory for influenza and RSV based on the original SKM described in Section 3.1. The background term was then simulated according to the generating model (12) and aggregate data and virological tests were generated according to (13) and (14) respectively. An illustration of the simulated data and posterior summaries are provided in the Supplement.

Though it is clear that the simulated aggregated data produces similar dynamics to what was observed in San Luis Potosí, México, the simulation fails to reproduce the larger spikes in number of aggregate cases that in our model are explained by secondary peaks of a given epidemic. A possible explanation for this phenomenon is the fact that multiple strains of each pathogen in circulation have different characteristics, which can only be recovered on average over a full year of real data. Therefore, simulating from this model would produce behaviour associated with such an "average" strain. Virological data appears to be well reproduced by the simulation model, although there may be evidence that unmodeled temporal correlation between these data could be present. For all the years being considered, the analysis of the simulated data yields results that were expected given the simulation settings. In particular, the order of the pathogen peaks and their location were correctly recovered, though the apparent overlap of peak infection for influenza with the initial peak in RSV in year 2005-2006 was not predicted. This may be explained by the fact that large initial epidemic peak in the real data for 2005-2006 was not reproduced in the simulated data, so that coincident infections were not required to explain the simulated data.

5.3 Identifiability in the Multi-pathogen Problem

In general, the ability to estimate parameters and distinguish pathogen dynamics depends on both the model structure and the availability and type of data used to estimate them (Huppert and Katriel 2013). Various features of this problem are known as identifiability, and have been studied in the context of infection models. Shrestha et al. (2011) show

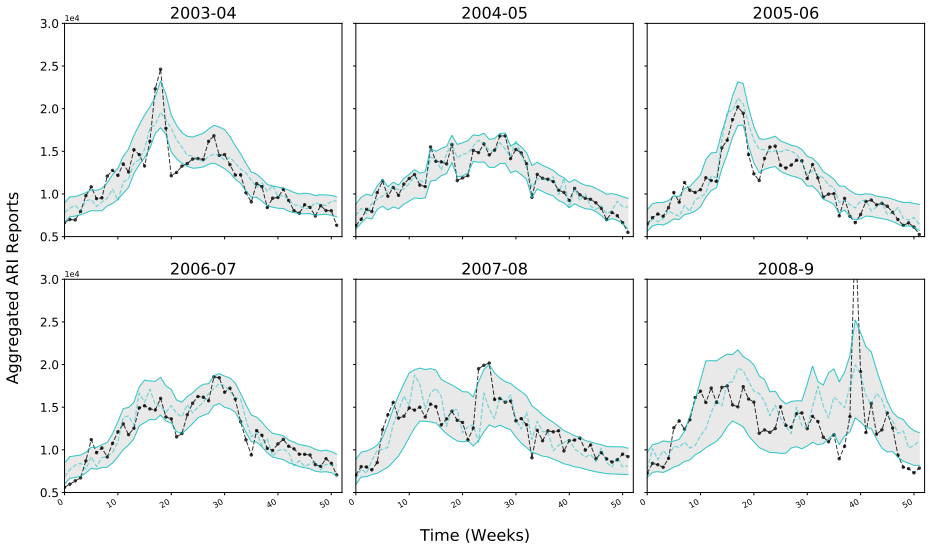

Figure 2: Posterior summaries for aggregated ARI reports from San Luis Potosí, México. The aggregated data, measured from August to July of the following year, is represented by black dots. Grey bands represent point-wise 95% credible intervals and the cyan dotted line shows a maximum a-posteriori estimated trajectory.

via simulation that likelihood-based methods can identify parameters of a multi-pathogen system under some conditions for models where the states are defined by a Multinomial process with expectation given by the solution of an ODE initial value problem. In a thorough investigation of sensitivity and local identifiability for SKMs, Komorowski et al. (2011) develop an approach to compute the Fisher Information Matrix for the model parameters, providing a valuable tool for model diagnosis. However, this approach is limited in our setting, because the order in which the individual epidemic trajectories peak is closely tied to the estimated initial states, which lie on the 8-simplex. Since traditionally used tools for diagnosing lack of identifiability are not directly applicable, simulation under different data availability scenarios can help to illustrate the value of

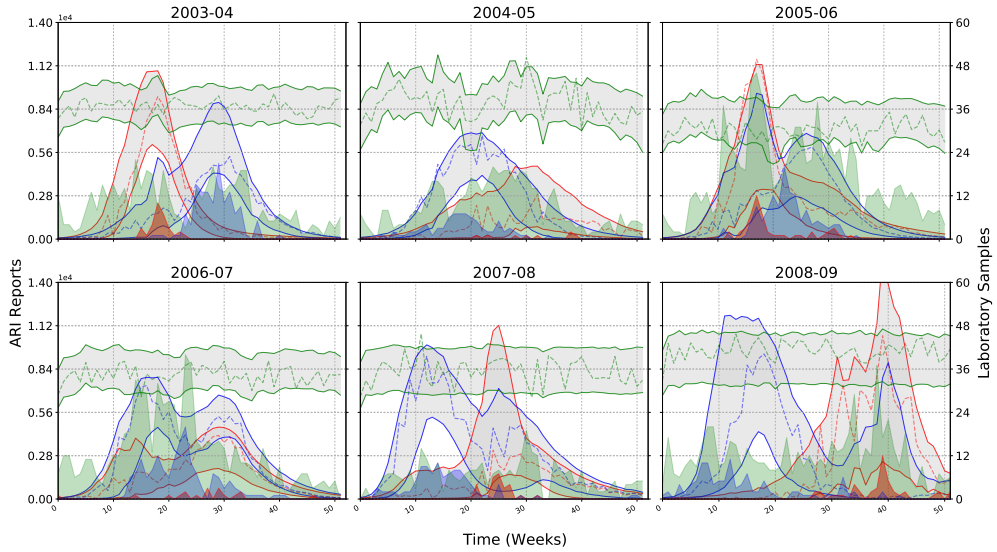

Figure 3: Posterior summaries for disaggregated reports based on data from San Luis Potosí, México. Left axis: Grey bands represent 95% credible intervals for influenza (red outline), RSV (blue outline) and background infections (green outline). Dotted lines represent maximum a-posteriori estimated trajectories. Right axis: Reports of influenza and RSV from ARI affected children under 5 years of age at Hospital Central, with tests positive for influenza, RSV, and neither, are shown as shaded red, blue, and green polygons, respectively.

additional virological data in identifying which is the leading epidemic in a given season. However, care must be taken in how these simulations are conducted, as direct comparison by removing the likelihood component corresponding to the additional virological data also removes the important constraint against over-fitting by the background infection model (12). Therefore, to illustrate the sensitivity of the model to lack of information on individual infections, we replace (12) with a linear discrepancy term to facilitate comparison. Figure 4 illustrates 25 posterior sample paths with (right panel) and without (left panel) including the virological data in the analysis of simulated data from 2003-04. Although most of the posterior sample paths for the model fitted using only aggregated reports point to influenza

as the first pathogen to peak over RSV (red lines dominate blue lines in the first peak), some uncertainty remains about their order[2]. On the other hand, including virological data induces a clear preference for influenza as the first pathogen to peak, although multiple smaller peaks for each epidemic may still be present.

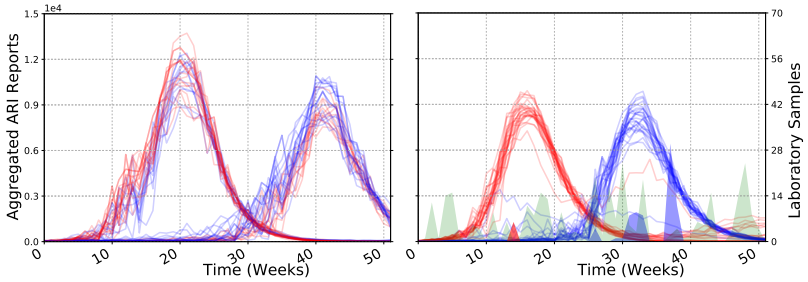

Figure 4: Left: 25 posterior sample paths over the trajectories of influenza (red) and RSV (blue) given aggregate ARI reports only. Right: 25 posterior sample paths over the trajectories of trajectories of influenza (red) and RSV (blue) given both the aggregated ARI reports and the virological test data. The virological test data is reported on the right axis of the figure, with tests positive for influenza, RSV, and neither, shown as shaded red, blue, and green polygons, respectively.

6 DISCUSSION

We have presented a Bayesian hierarchical model based on stochastic kinetic dynamics for two pathogens with similar symptoms and have extended the marginal sampling approach of Fearnhead et al. (2014) to integrate multiple data sources and include an empirically based discrepancy model representing infections with other pathogens. We found that the inclusion of the additional virological data allowed us to recover cross-interference parameters and to disaggregate the trajectories of individual pathogens. Our approach is

[2]This also highlights the importance of using population based sampling methods, such as Parallel Tempering MCMC, to enable exploration of multiple posterior modes.

general and can be applied to the problem of inference on stochastic kinetic models, as well as models of more than two interacting epidemics, when enough data is available to recover their individual dynamics.

Simulations suggest that our approach correctly recovers cross-immunities and the order and location of epidemic peaks of influenza and RSV in a given epidemic year. This is important because of the central role that cross-immunity plays in shaping the evolutionary and epidemiological dynamics of multi-strain pathogens (Gjini et al. 2016; Zhang et al. 2013). Changes in cross-immunity are known to give rise to complex temporal dynamics in disease incidence, and create oscillating time series from which it is difficult to estimate parameters that govern the underlying epidemiological processes (Reich et al. 2013; Bhattacharyya et al. 2015). Studies about relationship between influenza and RSV are predominantly qualitative (Pinky and Dobrovolny 2016; Bhattacharyya et al. 2015; Gröndahl et al. 2014). Though cross-immunities have been estimated for pathogens such as dengue (Reich et al. 2013) and influenza and pneumococcal pneumonia (Shrestha et al. 2013), to our knowledge, there have been no quantitative studies of cross-interference between influenza and RSV. Furthermore, to our knowledge, our work is the first to estimate cross-immunity parameters for an SKM.

The flexibility of our model to capture multiple epidemic peaks is useful. For example, Osthus et al. (2019) point out that a deterministic SIR model is restricted as to the number of peaks it can capture within a single season, and a dynamic discrepancy model is required to overcome this misspecification. As our model is stochastic, the posterior trajectories can indeed have multiple peaks. The background model we selected is purposely independent

of the influenza-RSV dynamics, but its flexibility is restricted to avoid confounding with the observation error process and to avoid over-fitting.

In future work we plan to address several questions. First, we believe that accounting for vaccination effects and seasonal forcing will yield additional insight into the interaction of these two pathogens. However, estimation of these additional model components will likely require the use of additional sources of data, such as vaccination reports and local climate variables collected in the state. Secondly, our analysis agrees with the fact that multiple strains of both influenza and RSV circulate during each year. Indeed, the emergence of very virulent strains, such as in April of 2009, is not suitably captured by our model in which parameters are essentially shared between strains of a single pathogen within each year. Therefore, modeling such strains as separate pathogens may yield better understanding of the circulation of ARI in the state.

These results can be of great use in epidemiological analyses that are carried out to estimate the burden of influenza on morbidity and mortality at local, national, or regional levels. Most current estimates of influenza-associated morbidity and mortality do not take into account the contribution of RSV to excess mortality, due mainly to the scarcity of virological surveillance information for all relevant viruses to incorporate in these analysis. Our findings provide evidence that maintaining a sentinel program, by administering virological tests at a clinical referral center, allows for reliable tracking of virus circulation time at the population level at a relatively low cost. Our analysis shows that even a relatively small number of such virological tests, when administered to all the patients in a particular group can help to provide information about patterns of pathogen

circulation.

References

Adams, B. and Boots, M. (2007). "The Influence of Immune Cross-Reaction on Phase Structure in Resonant Solutions of a Multi-Strain Seasonal SIR Model". *Journal of theoretical biology*, 248(1):202–211.

Allen, L. J. (2008). "An Introduction to Stochastic Epidemic Models". In *Mathematical epidemiology*, pages 81–130. Springer.

Anderson, L. J., Hierholzer, J. C., Tsou, C., Hendry, R. M., Fernie, B. F., Stone, Y., and McIntosh, K. (1985). Antigenic characterization of respiratory syncytial virus strains with monoclonal antibodies. *Journal of Infectious Diseases*, 151(4):626–633.

Ånestad, G. (1987). "Surveillance of Respiratory Viral Infections by Rapid Immunofluorescence Diagnosis, with Emphasis on Virus Interference". *Epidemiology and infection*, 99(02):523–531.

Anestad, G. et al. (1982). "Interference Between Outbreaks of Respiratory Syncytial Virus and Influenza Virus Infection". *Interference between outbreaks of respiratory syncytial virus and influenza virus infection.*, 1.

Anestad, G. and Nordbo, S. (2009). "Interference Between Outbreaks of Respiratory Viruses". *Euro Surveill*, 14(41):19359.

Australian Government Department of Health (2017). Australian influenza surveillance report.

Bhattacharyya, S., Gesteland, P. H., Korgenski, K., Bjørnstad, O. N., and Adler, F. R. (2015). Cross-immunity between strains explains the dynamical pattern of paramyxoviruses. *Proceedings of the National Academy of Sciences*, 112(43):13396–13400.

Bloom-Feshbach, K., Alonso, W. J., Charu, V., Tamerius, J., Simonsen, L., Miller, M. A., and Viboud, C. (2013). "Latitudinal Variations in Seasonal Activity of Influenza and Respiratory Syncytial Virus (RSV): a Global Comparative Review". *PloS one*, 8(2):e54445.

Boys, R. J., Wilkinson, D. J., and Kirkwood, T. B. (2008). Bayesian inference for a discretely observed stochastic kinetic model. *Statistics and Computing*, 18(2):125–135.

Brynjarsdóttir, J. and O'Hagan, A. (2014). Learning about physical parameters: the importance of model discrepancy. *Inverse Problems*, 30(11):114007.

Centers for Disease Control and Prevention (2008). Prevention and control of influenza recommendations of the advisory committee on immunization practices, 2008.

Chan, K. P., Wong, C. M., Chiu, S. S., Chan, K. H., Wang, X. L., Chan, E. L., Peiris, J. M., and Yang, L. (2014). "A Robust Parameter Estimation Method for Estimating Disease Burden of Respiratory Viruses". *PloS one*, 9(3):e90126.

Chaw, L., Kamigaki, T., Burmaa, A., Urtnasan, C., Od, I., Nyamaa, G., Nymadawa, P., and Oshitani, H. (2016). "Burden of Influenza and Respiratory Syncytial Virus Infection in Pregnant Women and Infants Under 6 Months in Mongolia: A Prospective Cohort Study". *PloS one*, 11(2):e0148421.

Choi, B. and Rempala, G. A. (2011). Inference for discretely observed stochastic kinetic networks with applications to epidemic modeling. *Biostatistics*, 13(1):153–165.

Dukic, V., Lopes, H. F., and Polson, N. G. (2012). "Tracking Epidemics With Google Flu Trends Data and a State-Space SEIR Model". *Journal of the American Statistical Association*, 107(500):1410–1426.

Farah, M., Birrell, P., Conti, S., and Angelis, D. D. (2014). Bayesian emulation and calibration of a dynamic epidemic model for A/H1N1 Influenza. *Journal of the American Statistical Association*, 109(508):1398–1411.

Fearnhead, P., Giagos, V., and Sherlock, C. (2014). "Inference for Reaction Networks Using the Linear Noise Approximation". *Biometrics*, 70(2):457–466.

Ferguson, N. M., Galvani, A. P., and Bush, R. M. (2003). Ecological and immunological determinants of influenza evolution. *Nature*, 422(6930):428.

Geyer, C. (1991). Markov chain Monte Carlo maximum likelihood. In *Computing Science and Statistics, Proceedings of the 23rd Symposium on the Interface, 156*. American Statistical Association.

Gillespie, D. T. (2007). "Stochastic Simulation of Chemical Kinetics". *Annu. Rev. Phys. Chem.*, 58:35–55.

Gjini, E., Valente, C., Sa-Leao, R., and Gomes, M. G. M. (2016). How direct competition shapes coexistence and vaccine effects in multi-strain pathogen systems. *Journal of theoretical biology*, 388:50–60.

Golightly, A., Henderson, D. A., and Sherlock, C. (2015). "Delayed Acceptance Particle MCMC for Exact Inference in Stochastic Kinetic Models". *Statistics and Computing*, 25(5):1039–1055.

Golightly, A. and Wilkinson, D. J. (2011). "Bayesian Parameter Inference for Stochastic Biochemical Network Models Using Particle Markov Chain Monte Carlo". *Interface Focus*.

Gómez-Villa, R., Comas-García, A., López-Rojas, V., Pérez-González, L., Sánchez-Alvarado, J., Salazar-Zaragoza, R., Ruiz-González, J., Alpuche-Solís, A., and Noyola, D. (2017). Effect of an infection control program on the frequency of nosocomial viral respiratory infections. *Infection Control & Hospital Epidemiology*, 29:556–558.

Grimshaw, R. (1991). *"Nonlinear Ordinary Differential Equations"*, volume 2. CRC Press.

Gröndahl, B., Ankermann, T., von Bismarck, P., Rockahr, S., Kowalzik, F., Gehring, S., Meyer, C., Knuf, M., and Puppe, W. (2014). The 2009 pandemic influenza a

(h1n1) coincides with changes in the epidemiology of other viral pathogens causing acute respiratory tract infections in children. *Infection*, 42(2):303–308.

Huppert, A. and Katriel, G. (2013). "Mathematical Modelling and Prediction in Infectious Disease Epidemiology". *Clinical Microbiology and Infection*, 19(11):999–1005.

Kamo, M. and Sasaki, A. (2002). "The Effect of Cross-Immunity and Seasonal Forcing in a Multi-Strain Epidemic Model". *Physica D: Nonlinear Phenomena*, 165(3):228–241.

Komorowski, M., Costa, M. J., Rand, D. A., and Stumpf, M. P. H. (2011). Sensitivity, robustness, and identifiability in stochastic chemical kinetics models. *Proceedings of the National Academy of Sciences*, 108(21):8645–8650.

Komorowski, M., Finkenstädt, B., Harper, C. V., and Rand, D. A. (2009). "Bayesian Inference of Biochemical Kinetic Parameters Using the Linear Noise Approximation". *BMC bioinformatics*, 10(1):1.

Kuri-Morales, P., Galván, F., Cravioto, P., Rosas, L. A. Z., and Tapia-Conyer, R. (2006). "Mortalidad en México por Influenza y Neumonía (1990-2005)". *Salud pública de México*, 48(5):379–384.

Mangtani, P., Hajat, S., Kovats, S., Wilkinson, P., and Armstrong, B. (2006). "The Association of Respiratory Syncytial Virus Infection and Influenza with Emergency Admissions for Respiratory Disease in London: an Analysis of Routine Surveillance Data". *Clinical infectious diseases*, 42(5):640–646.

Meskill, S., Revell, P., Chandramohan, L., and Cruz, A. (2017). Prevalence of co-infection between respiratory syncytial virus and influenza in children. *The American Journal of Emergency Medicine*, 35(3):495–498.

Mufson, M. A., Belshe, R. B., Örvell, C., and Norrby, E. (1988). Respiratory syncytial virus epidemics: variable dominance of subgroups a and b strains among children, 1981–1986. *Journal of Infectious Diseases*, 157(1):143–148.

Munywoki, P., C Koech, D., Agoti, C., Lewa, C., Cane, P., Medley, G., and Nokes, d. (2013). The source of respiratory syncytial virus infection in infants: A household cohort study in rural kenya. *The Journal of infectious diseases*, 209.

Osthus, D., Gattiker, J., Priedhorsky, R., and Del Valle, S. Y. (2019). Dynamic bayesian influenza forecasting in the United States with hierarchical discrepancy (with discussion). *Bayesian Anal.*, 14(1):261–312.

Peret, T., Hall, C. B., Schnabel, K. C., Golub, J. A., and Anderson, L. J. (1998). Circulation patterns of genetically distinct group a and b strains of human respiratory syncytial virus in a community. *Journal of General Virology*, 79(9):2221–2229.

Pinky, L. and Dobrovolny, H. M. (2016). Coinfections of the respiratory tract: viral competition for resources. *PLoS One*, 11(5):e0155589.

Rambaut, A., Pybus, O. G., Nelson, M. I., Viboud, C., Taubenberger, J. K., and Holmes, E. C. (2008). The genomic and epidemiological dynamics of human influenza a virus. *Nature*, 453(7195):615.

Reich, N. G., Shrestha, S., King, A. A., Rohani, P., Lessler, J., Kalayanarooj, S., Yoon, I.-K., Gibbons, R. V., Burke, D. S., and Cummings, D. A. (2013). Interactions between serotypes of dengue highlight epidemiological impact of cross-immunity. *Journal of The Royal Society Interface*, 10(86):20130414.

Shrestha, S., Foxman, B., Weinberger, D. M., Steiner, C., Viboud, C., and Rohani, P. (2013). Identifying the Interaction Between Influenza and Pneumococcal Pneumonia Using Incidence Data. *Science translational medicine*, 5(191).

Shrestha, S., King, A. A., and Rohani, P. (2011). "Statistical Inference for Multi-Pathogen Systems". *PLoS Comput Biol*, 7(8).

Siettos, C. I. and Russo, L. (2013). "Mathematical Modeling of Infectious Disease Dynamics". *Virulence*, 4(4):295–306.

Star, L. and Moghadas, S. (2010). "The Role of Mathematical Modelling in Public Health Planning and Decision Making". *Purple Paper. National Collaborative Center for Infectious Diseases. Issue*, (22).

Thomas, P., Matuschek, H., and Grima, R. (2012). "Intrinsic Noise Analyzer: a Software Package for the Exploration of Stochastic Biochemical Kinetics Using the System Size Expansion". *PloS one*, 7(6):e38518.

Thompson, W. W., Shay, D. K., Weintraub, E., Brammer, L., Cox, N., Anderson, L. J., and Fukuda, K. (2003). "Mortality Associated with Influenza and Respiratory Syncytial Virus in the United States". *Jama*, 289(2):179–186.

Troeger, C., Blacker, B., Khalil, I. A., Rao, P. C., Cao, J., Zimsen, S. R. M., Albertson, S. B., Deshpande, A., Farag, T., Abebe, Z., Adetifa, I. M. O., Adhikari, T. B., Akibu, M., Al Lami, F. H., Al-Eyadhy, A., Alvis-Guzman, N., Amare, A. T., Amoako, Y. A., Antonio, C. A. T., Aremu, O., Asfaw, E. T., Asgedom, S. W., Atey, T. M., Attia, E. F., Avokpaho, E. F. G. A., Ayele, H. T., Ayuk, T. B., Balakrishnan, K., Barac, A., Bassat, Q., Behzadifar, M., Behzadifar, M., Bhaumik, S., Bhutta, Z. A., Bijani, A., Brauer, M., Brown, A., Camargos, P. A. M., Castaeda-Orjuela, C. A., Colombara, D., Conti, S., Dadi, A. F., Dandona, L., Dandona, R., Do, H. P., Dubljanin, E., Edessa, D., Elkout, H., Endries, A. Y., Fijabi, D. O., Foreman, K. J., Forouzanfar, M. H., Fullman, N., Garcia-Basteiro, A. L., Gessner, B. D., Gething, P. W., Gupta, R., Gupta, T., Hailu, G. B., Hassen, H. Y., Hedayati, M. T., Heidari, M., Hibstu, D. T., Horita, N., Ilesanmi, O. S., Jakovljevic, M. B., Jamal, A. A., Kahsay, A., Kasaeian, A., Kassa, D. H., Khader, Y. S., Khan, E. A., Khan, M. N., Khang, Y.-H., Kim, Y. J., Kissoon, N., Knibbs, L. D., Kochhar, S., Koul, P. A., Kumar, G. A., Lodha, R., Magdy Abd El Razek, H., Malta, D. C., Mathew, J. L., Mengistu, D. T., Mezgebe, H. B., Mohammad, K. A., Mohammed, M. A., Momeniha, F., Murthy, S., Nguyen, C. T., Nielsen, K. R., Ningrum, D. N. A., Nirayo, Y. L., Oren, E., Ortiz, J. R., PA, M., Postma, M. J., Qorbani, M., Quansah, R., Rai, R. K., Rana, S. M., Ranabhat, C. L., Ray, S. E., Rezai, M. S., Ruhago, G. M., Safiri, S., Salomon, J. A., Sartorius, B., Savic, M., Sawhney, M., She, J., Sheikh, A., Shiferaw, M. S., Shigematsu, M., Singh, J. A., Somayaji, R., Stanaway, J. D., Sufiyan, M. B., Taffere, G. R., Temsah, M.-H., Thompson, M. J., Tobe-Gai, R., Topor-Madry, R., Tran, B. X., Tran, T. T., Tuem, K. B., Ukwaja, K. N., Vollset, S. E., Walson, J. L.,

Weldegebreal, F., Werdecker, A., West, T. E., Yonemoto, N., Zaki, M. E. S., Zhou, L., Zodpey, S., Vos, T., Naghavi, M., Lim, S. S., Mokdad, A. H., Murray, C. J. L., Hay, S. I., and Reiner, Jr, R. C. (2018). Estimates of the global, regional, and national morbidity, mortality, and aetiologies of lower respiratory infections in 195 countries, 19902016: a systematic analysis for the global burden of disease study 2016. *The Lancet Infectious Diseases*, 18(11):1191–1210.

Van Kampen, N. G. (1992). *"Stochastic Processes in Physics and Chemistry"*, volume 1. Elsevier.

Vasco, D. A., Wearing, H. J., and Rohani, P. (2007). "Tracking the Dynamics of Pathogen Interactions: Modeling Ecological and Immune-Mediated Processes in a Two-Pathogen Single-Host System". *Journal of Theoretical Biology*, 245(1):9–25.

Velasco-Hernández, J. X., Núñez-López, M., Comas-García, A., Cherpitel, D. E. N., and Ocampo, M. C. (2015). "Superinfection Between Influenza and RSV Alternating Patterns in San Luis Potosí State, México". *PloS one*, 10(3):e0115674.

Venter, M., Madhi, S. A., Tiemessen, C. T., and Schoub, B. D. (2001). Genetic diversity and molecular epidemiology of respiratory syncytial virus over four consecutive seasons in south africa: identification of new subgroup a and b genotypes. *Journal of General Virology*, 82(9):2117–2124.

Vizcarra-Ugalde, S., Rico-Hernández, M., Monjarás-Ávila, C., Bernal-Silva, S., Garrocho-Rangel, M., Ochoa-Pérez, U., and Noyola, D. (2016). Intensive care unit

admission and death rates of infants admitted with respiratory syncytial virus lower respiratory tract infection in Mexico. *The Pediatric Infectious Disease Journal*, 35(11):1199–1203.

Wikle, C. K. and Berliner, L. M. (2007). A bayesian tutorial for data assimilation. *Physica D: Nonlinear Phenomena*, 230(1):1 – 16.

Wilkinson, D. (2006). *"Stochastic Modelling for Systems Biology"*. Chapman & Hall/CRC Mathematical & Computational Biology. Taylor & Francis.

Wilkinson, D. (2011). *"Stochastic Modelling for Systems Biology, Second Edition"*. Chapman & Hall/CRC Mathematical and Computational Biology. Taylor & Francis.

World Health Organization (2017). [online]"Life Expectancy". `http://www.who.int/gho/mortality_burden_disease/life_tables/situation_trends/en/`.

Wu, Z., Sun, X., Chu, Y., Sun, J., Qin, G., Yang, L., Qin, J., Xiao, Z., Ren, J., Qin, D., Wang, X.-L., and Zheng, X. (2016). Coherence of influenza surveillance data across different sources and age groups, beijing, china, 2008-2015. *PLOS ONE*, 11:e0169199.

Zambon, M., Stockton, J., Clewley, J., and Fleming, D. (2001). Contribution of influenza and respiratory syncytial virus to community cases of influenza-like illness: an observational study. *The Lancet*, 358(9291):1410–1416.

Zhang, X.-S., De Angelis, D., White, P. J., Charlett, A., Pebody, R. G., and McCauley, J. (2013). Co-circulation of influenza a virus strains and emergence of pandemic via reassortment: the role of cross-immunity. *Epidemics*, 5(1):20–33.

7 APPENDIX

Algorithm 1: Approximate SMC algorithm targeting (15) for fixed (θ, τ)

Define the augmented state vector $\tilde{X} = [X^\top, D]^\top$ and observation vector $\tilde{G} = [G^\top, 1]^\top$. Define the matrix $\tilde{V}_i = \begin{bmatrix} V_i & 0 \\ 0 & V_i^d \end{bmatrix}$ initialized with $V_0 = \Omega c_0 \mathbb{I}_{\dim(X),\dim(X)}$ and $V_0^d = \Omega^{3/2}\kappa$. Define the vector $\tilde{m}_i = [m_i, m_i^d]^\top$ initialized with $m_0 = x_1^\top$ and $m_0^d = \Omega c$. Compute prior marginal likelihood:

$$p_a(y_1 \mid \theta, \tau) = \mathcal{N}\left(y_1; r\tilde{G}^\top \tilde{m}_0, r^2\tilde{G}^\top \tilde{V}_0 \tilde{G} + \Omega^2\Sigma\right)$$

The analysis distribution at time $t = 1$ is $p\left(\tilde{x}_1 \mid y_1\right) = \mathcal{N}\left(\tilde{x}_1; \tilde{m}_1, \tilde{V}_1\right)$ where

$$\tilde{m}_1 = \tilde{m}_0 + r\tilde{G}^\top \tilde{V}_0 (r\tilde{G}^T \tilde{V}_0 \tilde{G} + \Omega^2\Sigma)^{-1}\left(y_1 - r\tilde{G}^T \tilde{m}_0\right)$$
$$\tilde{V}_1 = \tilde{V}_0 - r^2\tilde{G}^\top \tilde{V}_0 (r^2\tilde{G}^\top \tilde{V}_0 \tilde{G} + \Omega^2\Sigma)^{-1}\tilde{V}_0 \tilde{G}$$

for i=1, ..., $M-1$ **do**

Integrate equations (4) and (9) from time t_i to t_{i+1} using as initial conditions $\phi_i = m_i/\Omega$ and $C_i = V_i/\Omega$, to obtain ϕ_{i+1} and C_{i+1}. Augment $\tilde{\phi}_{i+1} = [\phi_{i+1}^\top, c + m_i^d]^\top$ and $\tilde{C}_{i+1} = \begin{bmatrix} C_{i+1} & 0 \\ 0 & \Omega^{1/2}\kappa \end{bmatrix}$. The filtering distribution of $\tilde{X}$ is:

$$p_a\left(\tilde{x}_{i+1} \mid y_i\right) = \mathcal{N}\left(\tilde{x}_{i+1}; \Omega\tilde{\phi}_{i+1}, \Omega\tilde{C}_{i+1}\right)$$

Compute the marginal likelihood of Y_{i+1}:

$$p_a(y_{i+1} \mid \theta, \tau) = p_a\left(y_i \mid \theta, \tau\right) p_a\left(y_{i+1} \mid y_{1:i}\right)$$

where, $p_a\left(y_{i+1} \mid y_{1:i}\right) = \mathcal{N}\left(y_{i+1}; r\Omega\tilde{G}^\top \tilde{\phi}_{i+1}, r^2\Omega\tilde{G}^\top \tilde{C}_{i+1}\tilde{G} + \Omega^2\Sigma\right)$

The approximate analysis distribution at time t_{i+1} is $p_a\left(\tilde{x}_{i+1} \mid y_{1:i+1}\right) = \mathcal{N}\left(\tilde{x}_{i+1}; \tilde{m}_{i+1}, \tilde{V}_{i+1}\right)$ where

$$\tilde{m}_{i+1} = \Omega\phi_{i+1} + r\Omega\tilde{G}^\top \tilde{C}_0 (r\Omega\tilde{G}^T \tilde{C}_{i+1}\tilde{G} + \Omega^2\Sigma)^{-1}\left(y_{i+1} - r\Omega\tilde{G}^T \phi_{i+1}\right)$$
$$\tilde{V}_{i+1} = \Omega\tilde{C}_{i+1} - r^2\Omega^2\tilde{G}^\top \tilde{C}_{i+1}(r^2\Omega\tilde{G}^\top \tilde{C}_{i+1}\tilde{G} + \Omega^2\Sigma)^{-1}\tilde{C}_{i+1}\tilde{G}$$

Backward recursion, together with the approximation used to obtain the analysis distribution above leads to a smoothing distribution for $\tilde{X}_{1:M}$ equal to the approximate analysis distribution:

$$p_a\left(\tilde{x}_{1:M} \mid y_{1:M}\right) = \mathcal{N}\left(\tilde{x}_{1:M};\, \tilde{m}_{1:M}, \tilde{V}_{1:M}\right)$$

Sample a realization of $\tilde{x}_{1:M} = [x_{1:M}, d_{1:M}]$ from $p_a\left(\tilde{x}_{1:M} \mid y_{1:M}\right)$ and compute the likelihood component $p\left(n_{1:M} \mid x_{1:M}, d_{1:M}, y_{1:M}, \theta, \tau\right)$ from (14).

Return the product $p_a\left(y_{1:M} \mid \theta, \tau\right) p\left(n_{1:M} \mid x_{1:M}, d_{1:M}, y_{1:M}, \theta, \tau\right)$ together with associated sample path $\tilde{x}_{1:M}$.

8 SUPPLEMENTARY MATERIALS

Supplementary Material: "Inference for stochastic kinetic models from multiple data sources for joint estimation of infection dynamics from aggregate reports and virological data". This document contains details of the equations and matrix specification, as well as posterior summaries for the analysis of the real data and the simulations. (pdf)

Python code: All software has been uploaded for review purposes (GNU zipped tar file). Upon publication the code used to carry out the analysis will be provided online

Data: All data has been uploaded for review purposes (GNU zipped tar file) and will be made available as described in the JASA ACS Author Form.

Supplementary Material: Inference for stochastic kinetic models from multiple data sources for joint estimation of infection dynamics from aggregate reports and virological data

Yury E. García*, Oksana A. Chkrebtii*, Marcos A. Capistrán, Daniel E. Noyola

December 15, 2024

1 MODEL

This section provides mathematical details for the two-pathogen SIR model considered in the paper "Inference for stochastic kinetic models from multiple data sources for joint estimation of infection dynamics from aggregate reports and virological data".

*These authors contributed equally

1.1 Chemical Master Equation

We define a stochastic SIR model for two pathogens following Kamo and Sasaki (2002). Let,

$$X(t) = [X_{SS}(t), X_{IS}(t), X_{RS}(t), X_{SI}(t), X_{RI}(t), X_{SR}(t), X_{IR}(t)]^\top,$$

where $X_{kl}(t)$ denotes the number of individuals at time t in immunological status $k \in \{S, I, R\}$ for pathogen 1 (influenza) and immunological status $l \in \{S, I, R\}$ for pathogen 2 (RSV). Vector $x(t)$ corresponds to the realization of the random vector $X(t)$. Reactions associated with these events are listed in Table 1, where $\lambda_1 = (x_{is} + x_{ir})/\Omega$ is the proportion of individuals infected with pathogen 1, and $\lambda_2 = (x_{si} + x_{ri})/\Omega$ is the proportion infected with pathogen 2. The number of possible reaction is $\mathcal{R} = 17$. The evolution of the probability distribution of finding the system in state x at time t is governed by the master equation,

$$\frac{dp_x(t)}{dt} = \sum_{i_1}^{\mathcal{R}} a_i(x - v_i)p_{x-v_i}(t) - \sum_{i=1}^{\mathcal{R}} a_i(x)p_x(t), \tag{1}$$

where v_i is the stoichiometric vector and a_i is the rate of reaction $i = 1, \ldots, 17$.

1.2 Large Volume Approximation

The van Kampen expansion (Van Kampen 1992) provides a large volume approximation to the solution of the master equation that is made up of two terms, as follows:

$$X(t) = \Omega\phi(t) + \Omega^{1/2}\xi(t), \tag{2}$$

Table 1: All possible reactions in the system; v_i is the stochiometric vector, and $a_i(x)$ is the propensity for the ith reaction, $i = 1, \ldots, 17$.

Reactions	**Propensity**	**Stoichiometric vector**
$\mu \to X_{SS}$	$a_1(x) = \mu\Omega + o(\Delta t)$	$v_1 = [1,0,0,0,0,0,0,0]$
$X_{SS} \to X_{SI}$	$a_2(x) = \beta_2\lambda_2 x_{ss} + o(\Delta t)$	$v_2 = [-1,0,0,1,0,0,0,0]$
$X_{SS} \to X_{IS}$	$a_3(x) = \beta_1\lambda_1 x_{ss} + o(\Delta t)$	$v_3 = [-1,1,0,0,0,0,0,0]$
$X_{SS} \to \mu$	$a_4(x = \mu x_{ss} + o(\Delta t)$	$v_4 = [-1,0,0,0,0,0,0,0]$
$X_{IS} \to \mu$	$a_5(x) = \mu x_{is} + o(\Delta t)$	$v_5 = [0,-1,0,0,0,0,0,0]$
$X_{IS} \to X_{RS}$	$a_6(x) = \gamma x_{is} + o(\Delta t)$	$v_6 = [0,-1,1,0,0,0,0,0]$
$X_{RS} \to \mu$	$a_7(x) = \mu x_{rs} + o(\Delta t)$	$v_7 = [0,0,-1,0,0,0,0,0]$
$X_{RS} \to X_{RI}$	$a_8(x) = \sigma\beta_2\lambda_2 x_{rs} + o(\Delta t)$	$v_8 = [0,0,-1,0,1,0,0,0]$
$X_{SI} \to X_{SR}$	$a_9(x) = \gamma x_{si} + o(\Delta t)$	$v_9 = [0,0,0,-1,0,1,0,0]$
$X_{SI} \to \mu$	$a_{10}(x) = \mu x_{si} + o(\Delta t)$	$v_{10} = [0,0,0,-1,0,0,0,0]$
$X_{RI} \to X_{RR}$	$a_{11}(x) = \gamma x_{ri} + o(\Delta t)$	$v_{11} = [0,0,0,0,-1,0,0,1]$
$X_{RI} \to \mu$	$a_{12}(x) = \mu x_{ri} + o(\Delta t)$	$v_{12} = [0,0,0,0,-1,0,0,0]$
$X_{SR} \to \mu$	$a_{13}(x) = \mu x_{sr} + o(\Delta t)$	$v_{13} = [0,0,0,0,0,-1,0,0]$
$X_{SR} \to X_{IR}$	$a_{14}(x) = \sigma\beta_1\lambda_1 x_{sr} + o(\Delta t)$	$v_{14} = [0,0,0,0,0,-1,1,0]$
$X_{IR} \to \mu$	$a_{15}(x) = \mu x_{ir} + o(\Delta t)$	$v_{15} = [0,0,0,0,0,0,-1,0]$
$X_{IR} \to X_{RR}$	$a_{16}(x) = \gamma x_{ir} + o(\Delta t)$	$v_{16} = [0,0,0,0,0,0,-1,1]$
$X_{RR} \to \mu$	$a_{17}(x) = \mu x_{rr} + o(\Delta t)$	$v_{17} = [0,0,0,0,0,0,0,-1]$

where $\phi(t)$ describes macroscopic behavior and ξ is the noise term representing the aggregate effects of demographic stochasticity on the system and describing its fluctuations. We make an expansion in the powers of Ω (Van Kampen 1992) and collect powers of $\Omega^{1/2}$ to get the macroscopic law given by the initial value problem,

$$\begin{cases} \dfrac{d\phi_i(t)}{dt} &= \sum_{j=1}^{\mathcal{R}} S_{ij} a_j(\phi(t)), \quad t \in (0,T],\ i = 1, \ldots, \dim\{X(t)\}, \\ \phi_i(0) &= \phi_0, \qquad\qquad\qquad\quad i = 1, \ldots, \dim\{X(t)\}. \end{cases} \tag{3}$$

Here $S = [v_1, \ldots, v_{\mathcal{R}}]$ is the stoichiometric matrix and $a(\phi) = [a_1(\phi), \ldots, a_{\mathcal{R}}(\phi)]$ is the vector of propensities. The full expressions for the macroscopic equations in the first line of (3) are:

$$\begin{aligned}
\frac{d\phi_0(t)}{dt} &= \mu - \beta_2\lambda_2\phi_0 - \beta_1\lambda_1\phi_0 - \mu\phi_0, \\
\frac{d\phi_1(t)}{dt} &= \beta_1\lambda_1\phi_0 - \gamma\phi_1 - \mu\phi_1, \\
\frac{d\phi_2(t)}{dt} &= \gamma\phi_1 - \sigma_2\beta_2\lambda_2\phi_2 - \mu\phi_2, \\
\frac{d\phi_3(t)}{dt} &= \beta_2\lambda_2\phi_0 - \gamma\phi_3 - \mu\phi_3, \\
\frac{d\phi_4(t)}{dt} &= \sigma_2\beta_2\lambda_2\phi_2 - \gamma\phi_4 - \mu\phi_4, \\
\frac{d\phi_5(t)}{dt} &= \gamma\phi_3 - \mu\phi_5 - \sigma_1\beta_1\lambda_1\phi_5, \\
\frac{d\phi_6(t)}{dt} &= -\gamma\phi_6 + \sigma_1\beta_1\lambda_1\phi_5 - \mu\phi_6, \\
\frac{d\phi_7(t)}{dt} &= \gamma\phi_6 + \gamma\phi_4 - \mu\phi_7.
\end{aligned} \tag{4}$$

The stochastic process ξ is governed by the Itô diffusion equation,

$$d\xi(t) = A(t)\xi(t)dt + \sqrt{B(t)}dW(t), \quad t \in [0, T], \tag{5}$$

$W(t)$ denotes the $\mathcal{R}$ dimensional Wiener process. Matrix $A(t)$ is given by $A(t) = \dfrac{\partial S\, a(\phi(t))}{\partial\phi(t)}$, and matrix $B(t)$ by $B = S\mathrm{diag}\left(a(\phi)\right) S^T$ (Van Kampen 1992; Gillespie 2007). Expressions for both matrices are provided in Table 2.

Table 2: Matrices defining the diffusion approximation of the master equation.

Matrix A

$$\begin{bmatrix}
-(\beta_2\lambda_2+\beta_1\lambda_1+\mu) & -\beta_1\phi_0 & 0 & -\beta_2\phi_0 & -\beta_2\phi_0 & 0 & -\beta_1\phi_0 & 0 \\
\beta_1\lambda_1 & \beta_1\phi_0-(\gamma+\mu) & 0 & 0 & 0 & 0 & \beta_1\phi_0 & 0 \\
0 & \gamma & -(\beta_2\lambda_2\sigma_2+\mu) & -\beta_2\phi_2\sigma_2 & -\beta_2\phi_2\sigma_2 & 0 & 0 & 0 \\
\beta_2\lambda_2 & 0 & 0 & \beta_2\phi_0-(\gamma+\mu) & \beta_2\phi_0 & 0 & 0 & 0 \\
0 & 0 & \beta_2\lambda_2\sigma_2 & \beta_2\sigma\phi_2 & \beta_2\sigma_2\phi_2-(\gamma+\mu) & 0 & 0 & 0 \\
0 & -\beta_1\phi_5\sigma_1 & 0 & \gamma & 0 & -\beta_1\lambda_1\sigma_1-\mu & -\beta_1\sigma_1\phi_5 & 0 \\
0 & \beta_1\sigma_1\phi_5 & 0 & 0 & 0 & \beta_1\lambda_1\sigma_1 & \beta_1\sigma_1\phi_5-(\gamma+\mu) & 0 \\
0 & 0 & 0 & 0 & \gamma & 0 & \gamma & -\mu
\end{bmatrix}$$

Matrix B

$$\begin{bmatrix}
\beta_2\lambda_2\phi_0+ & & & & & & & \\
\beta_1\lambda_1\phi_0+ & -\beta_1\phi_0\lambda_1 & & -\beta_2\lambda_2\phi_0 & 0 & 0 & 0 & 0 \\
\phi_0\mu+\mu & & & & & & & \\
-\beta_1\lambda_1\phi_0 & \beta_1\lambda_1\phi_0+\phi_1(\gamma+\mu) & -\gamma\phi_1 & 0 & 0 & 0 & 0 & 0 \\
0 & -\gamma\phi_1 & \gamma\phi_1+ & & & & & \\
 & & \beta_2\phi_2\lambda_2\sigma_2+\mu\phi_2 & 0 & -\beta_2\phi_2\lambda_2\sigma_2 & 0 & 0 & 0 \\
-\beta_2\phi_0\lambda_2 & 0 & 0 & \beta_2\phi_0\lambda_2+\phi_3(\gamma+\mu) & 0 & -\gamma\phi_3 & 0 & 0 \\
 & & & & \phi_4(\gamma+\mu) & & & \\
0 & 0 & -\beta_2\lambda_2\sigma_2\phi_2 & & \beta_2\lambda_2\sigma_2\phi_2 & 0 & 0 & -\gamma\phi_4 \\
0 & 0 & 0 & -\gamma\phi_3 & 0 & \gamma\phi_3+\mu\phi_5 & & \\
 & & & & & \beta_1\lambda_1\sigma_1\phi_5 & -\beta_1\phi_5\lambda_1\sigma_1 & 0 \\
0 & 0 & 0 & 0 & 0 & -\beta_1\sigma_1\lambda_1\phi_5 & \beta_1\lambda_1\sigma_1\phi_5 & \\
 & & & & & & (\gamma+\mu)\phi_6 & -\gamma\phi_6 \\
0 & 0 & 0 & 0 & -\gamma\phi_4 & 0 & -\gamma\phi_6 & \gamma\phi_4+ \\
 & & & & & & & \gamma\phi_6+\mu\phi_7
\end{bmatrix}$$

2 NUMERICAL RESULTS

This section provides posterior summaries and pairwise correlation plots from the analysis of real data (tables) and simulated data (figures) for each of the six epidemic years 2003-04 to 2008-09. The analysis was implemented Python. Python module "corner" (Foreman-Mackey 2016) used to display the bivariate posterior correlation plots.

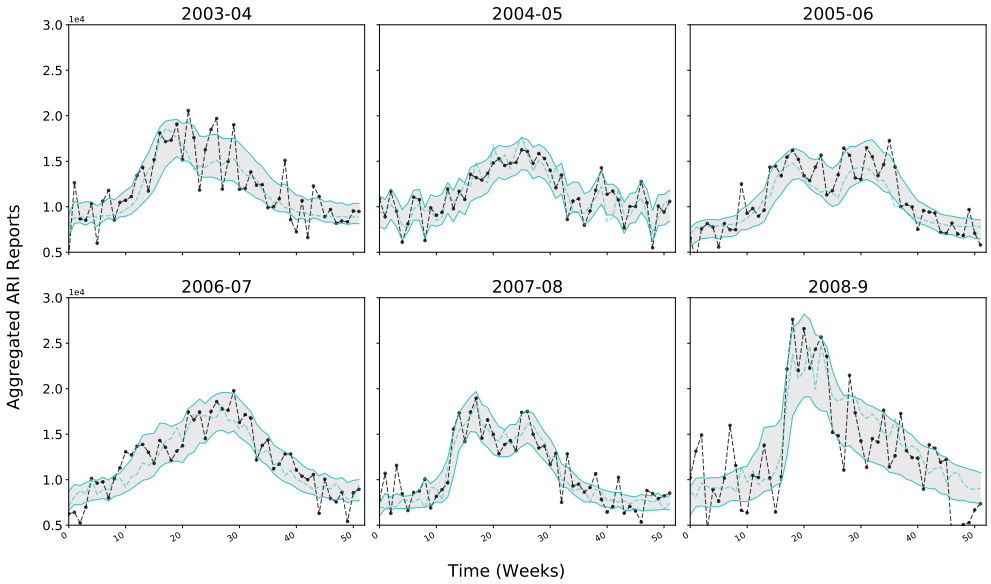

Figure 1: Posterior summaries for aggregated ARI reports from simulated data. The aggregated data, measured from August to July of the following year, is represented by black dots. Grey bands represent point-wise 95% credible intervals and the cyan dotted line shows a maximum a-posteriori estimated trajectory.

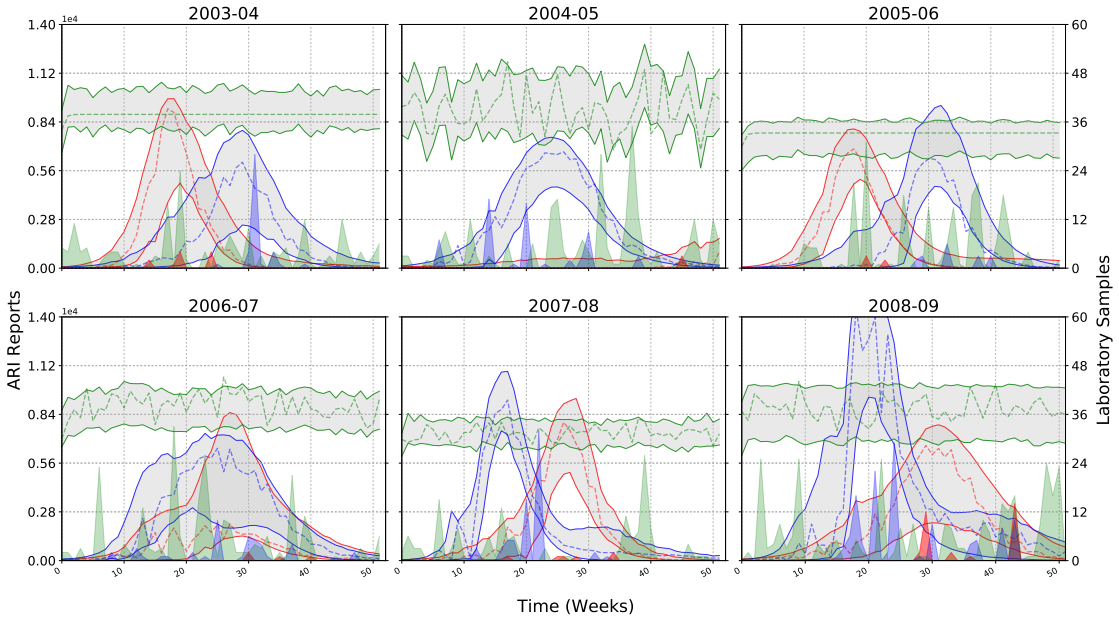

Figure 2: Posterior summaries for disaggregated reports based on simulated data. Left axis: Grey bands represent 95% credible intervals for influenza (red outline), RSV (blue outline) and background infections (green outline). Dotted lines represent maximum a-posteriori estimated trajectories. Right axis: Reports of influenza and RSV from ARI affected children under 5 years of age at Hospital Central, with tests positive for influenza, RSV, and neither, are shown as shaded red, blue, and green polygons, respectively.

August 2003 - July 2004

Table 3: Posterior summaries for the year 2003-04

Parameter	MAP	95% CIs	Parameter	MAP	95% CIs
β_1	82.888	(68.336, 84.998)	X_{SS}	2281950	(2272925, 2316750)
β_2	68.611	(52.863, 60.567)	X_{IS}	112	(6, 1646)
σ_1	0.55731	(0.062984, 3.8505)	X_{RS}	42207	(27147, 70475)
σ_2	1.8026	(1.6379, 2.3865)	X_{SI}	120	(982, 8988)
C_0	1.1532e-04	(2.1151e-04, 1.4881e-02)	X_{RI}	153	(705, 8590)
Σ	6.2585e-07	(4.5941e-07, 5.9472e-07)	X_{SR}	27767	(1298 26482)
r	0.07439	(0.07873, 0.09002)	X_{IR}	260	(21, 1214)
c	0.03758	(0.03185, 0.03435)	X_{RR}	147422	(119542, 160572)
ν	0.2002	(0.20092, 0.20318)			
v	0.1040	(0.1016, 0.10309)			

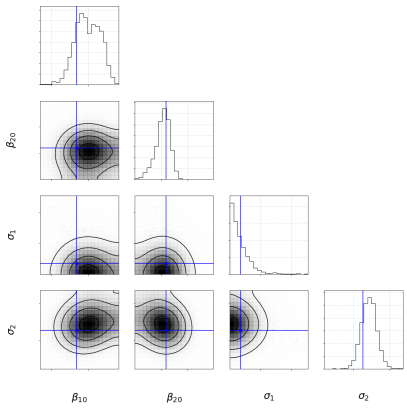

Figure 3: Analysis based on simulated data. Pairwise marginal contours for the parameters defining the stochastic kinetic model. Blue lines represent the values of the simulation parameters for comparison.

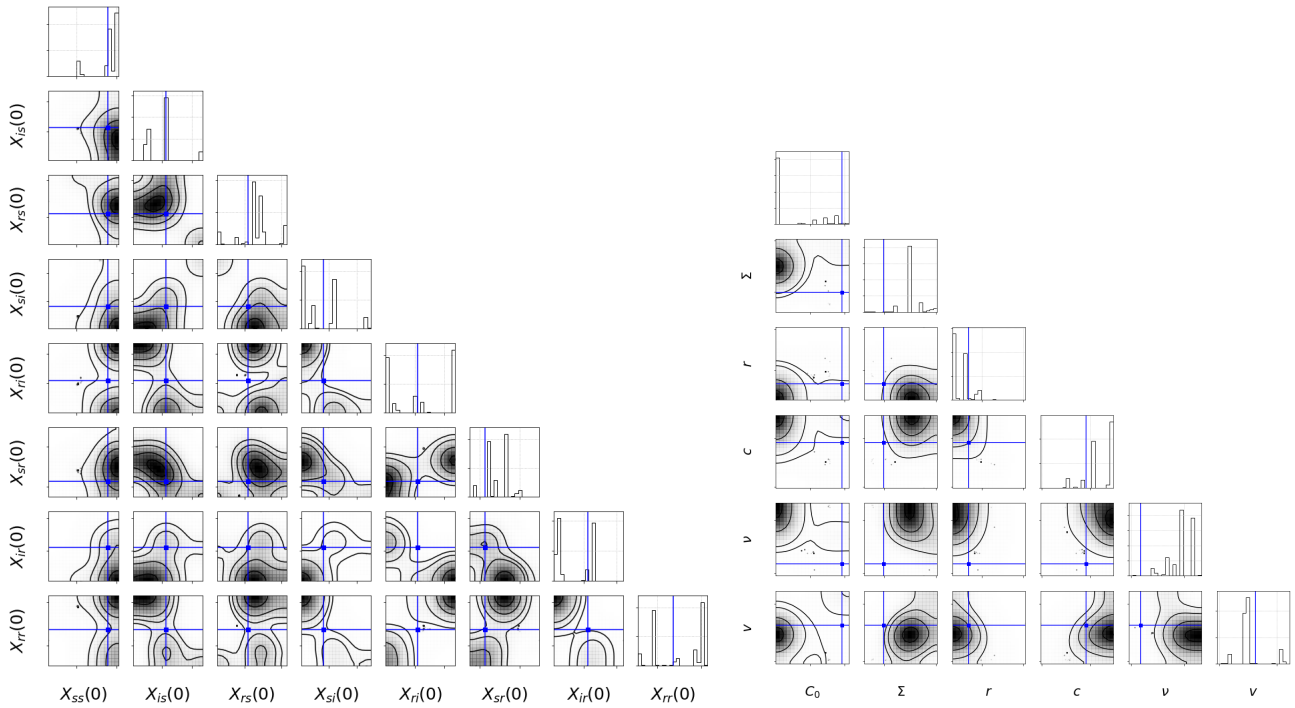

Figure 4: Analysis based on simulated data. Pairwise marginal contours for the initial conditions (left) and the auxiliary parameters (right). Blue lines represent the values of the simulation parameters for comparison.

August 2004 - July 2005

Table 4: Posterior summaries for the year 2004-05

Parameter	MAP	95% CIs	Parameter	MAP	95% CIs
β_1	64.3754	(50.2483, 71.1815)	X_{SS}	2281352	(2252426, 2284653)
β_2	68.3774	(58.2333, 69.3508)	X_{IS}	397	(45, 3809)
σ_1	1.4021	(0.4856, 3.2505)	X_{RS}	39800	(32530, 41698)
σ_2	1.5325	(0.5249, 6.5877)	X_{SI}	1880	(121, 9308)
C_0	8.8445e-03	(8.8445e-03, 1.6631e-02)	X_{RI}	2125	(84, 4770)
Σ	2.3857e-07	(2.0714e-07, 3.7927e-07)	X_{SR}	30237	(20542, 45622)
r	0.1035	(0.1009, 0.1275)	X_{IR}	455	(46, 13053)
c	0.02456	(0.02207, 0.02692)	X_{RR}	143751	(140067, 159271)
ν	0.1994	(0.1994, 0.2016)			
υ	0.0996	(0.09621, 0.09985)			

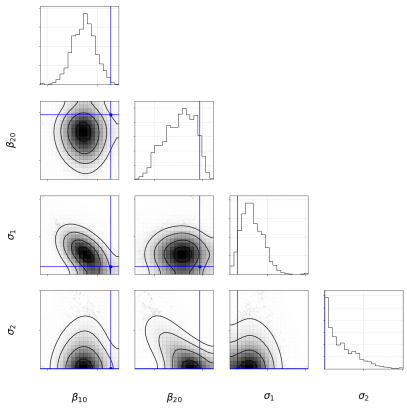

Figure 5: Analysis based on simulated data. Pairwise marginal contours for the parameters defining the stochastic kinetic model. Blue lines represent the values of the simulation parameters for comparison.

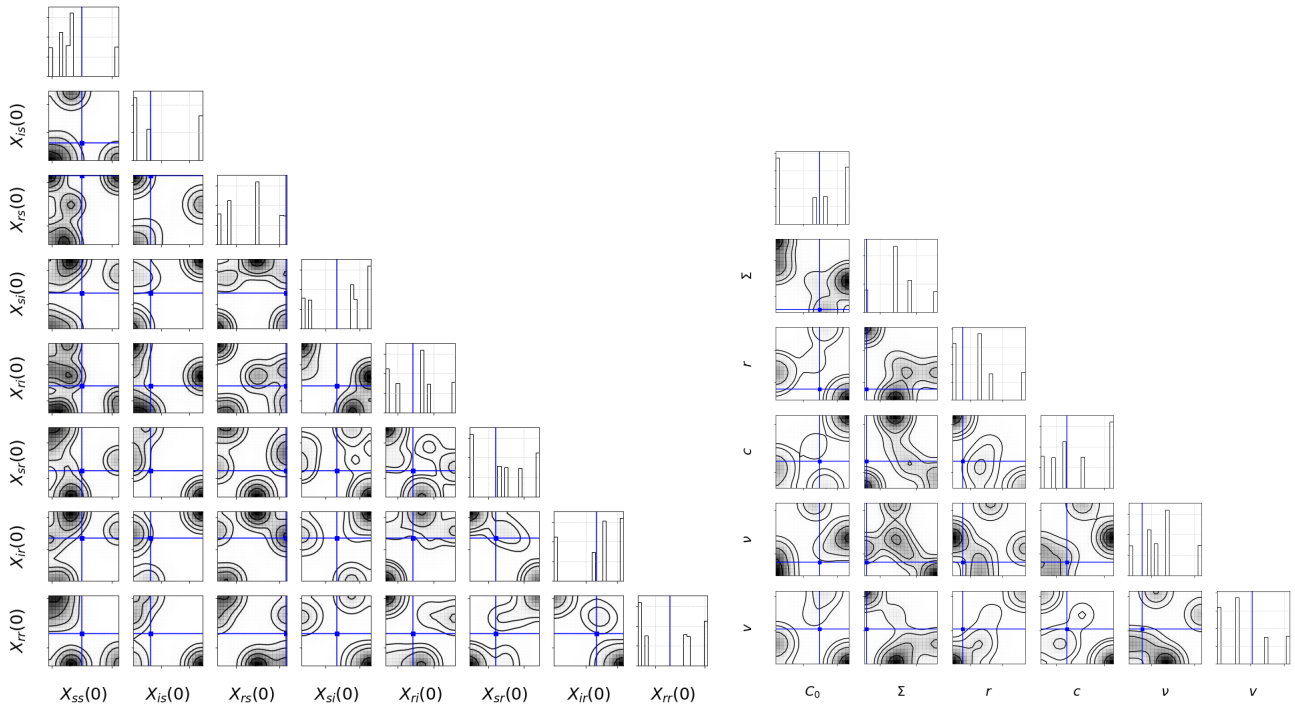

Figure 6: Analysis based on simulated data. Pairwise marginal contours for the initial conditions (left) and the auxiliary parameters (right). Blue lines represent the values of the simulation parameters for comparison.

August 2005 - July 2006

Table 5: Posterior summaries for the year 2005-06

Parameter	MAP	95% CIs	Parameter	MAP	95% CIs
β_1	42.0182	(29.6829, 70.7165)	X_{SS}	2280677	(2260296, 2308459)
β_2	60.8559	(57.2093, 64.5793)	X_{IS}	172	(60, 8445)
σ_1	1.433	(0.8806, 2.4955)	X_{RS}	52842	(46354, 65694)
σ_2	3.1773	(1.5288, 4.8721)	X_{SI}	523	(17, 10064)
C_0	2.1307e-03	(2.1264e-03, 2.0333e-02)	X_{RI}	10998	(458, 9972)
Σ	3.4695e-07	(2.3463e-07, 4.0426e-07)	X_{SR}	8511	(5143, 34599)
r	0.07464	(0.07464, 0.1026)	X_{IR}	3294	(121, 6687)
c	0.03248	(0.02310 0.03248)	X_{RR}	142980	(89822, 147742)
ν	0.2030	(0.1986, 0.2037)			
υ	0.0996	(0.0991, 0.1007)			

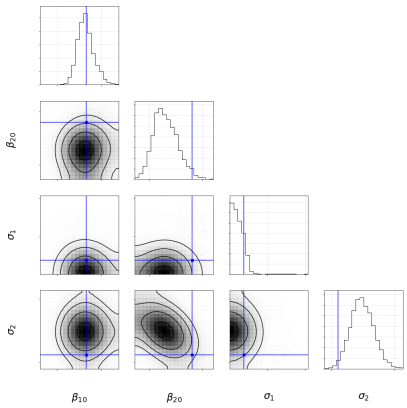

Figure 7: Analysis based on simulated data. Pairwise marginal contours for the parameters defining the stochastic kinetic model. Blue lines represent the values of the simulation parameters for comparison.

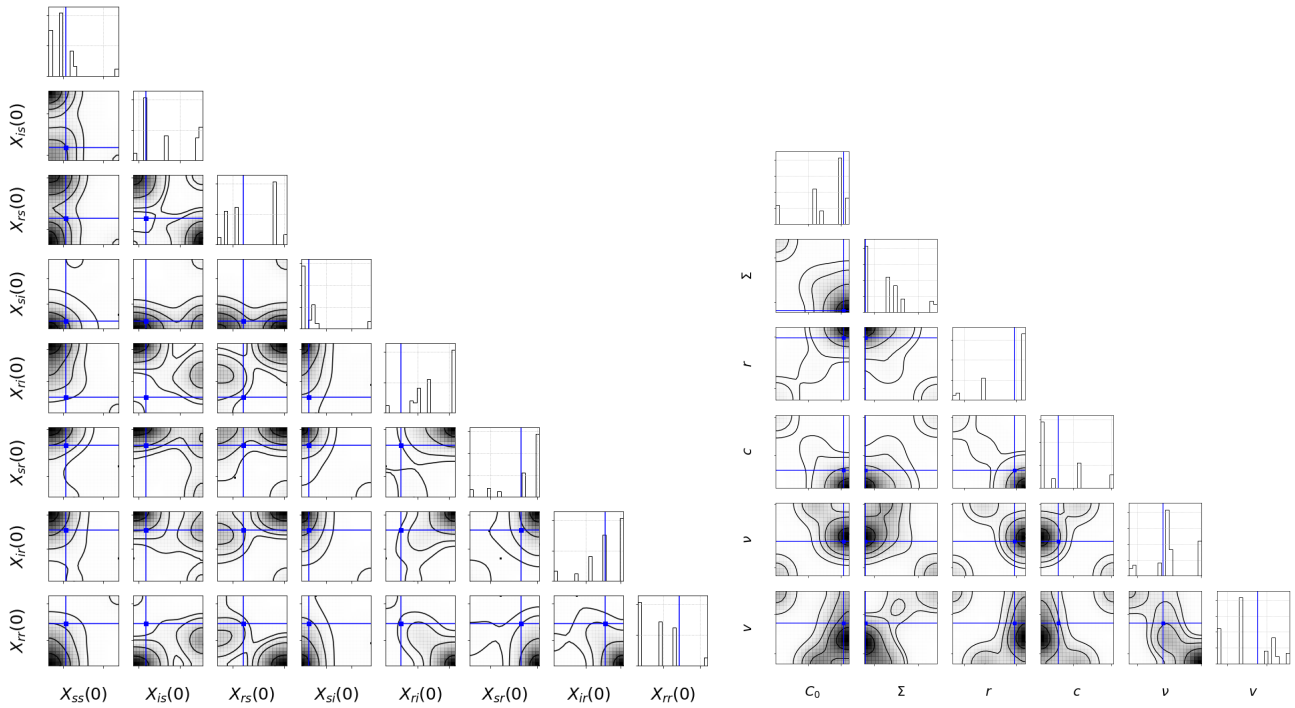

Figure 8: Analysis based on simulated data. Pairwise marginal contours for the initial conditions (left) and the auxiliary parameters (right). Blue lines represent the values of the simulation parameters for comparison.

August 2006 - July 2007

Table 6: Posterior summaries for the year 2006-07

Parameter	MAP	95% CIs	Parameter	MAP	95% CIs
β_1	65.0052	(51.6991, 72.5779)	X_{SS}	2283027	(2276015, 2283448)
β_2	65.9325	(59.1039, 72.71007)	X_{IS}	253	(22, 4565)
σ_1	1.2071	(0.7281, 2.9201)	X_{RS}	40492	(32380 , 44181)
σ_2	1.9023	(1.7082, 5.7772)	X_{SI}	1072	(529, 2642)
C_0	9.1189e-03	(9.7820e-03, 1.0184e-02)	X_{RI}	98	(228, 4203)
Σ	2.8170e-07	(2.5109e-07, 3.0907e-07)	X_{SR}	27489	(22628, 29628)
r	0.3452	(0.08717, 0.1061)	X_{IR}	69	(33, 6063)
c	7.6224e-03	(2.5762e-03 2.8315e-02)	X_{RR}	147496	(142788, 149660)
ν	0.1999	(0.1999, 0.2000)			
υ	0.10005	(0.1000, 0.1001)			

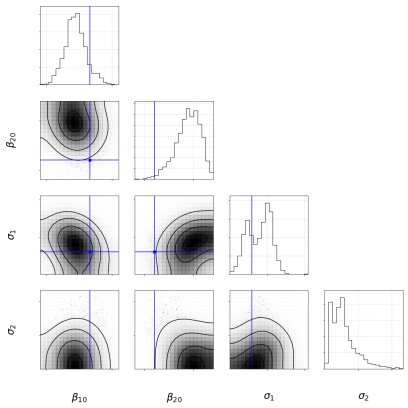

Figure 9: Analysis based on simulated data. Pairwise marginal contours for the parameters defining the stochastic kinetic model. Blue lines represent the values of the simulation parameters for comparison.

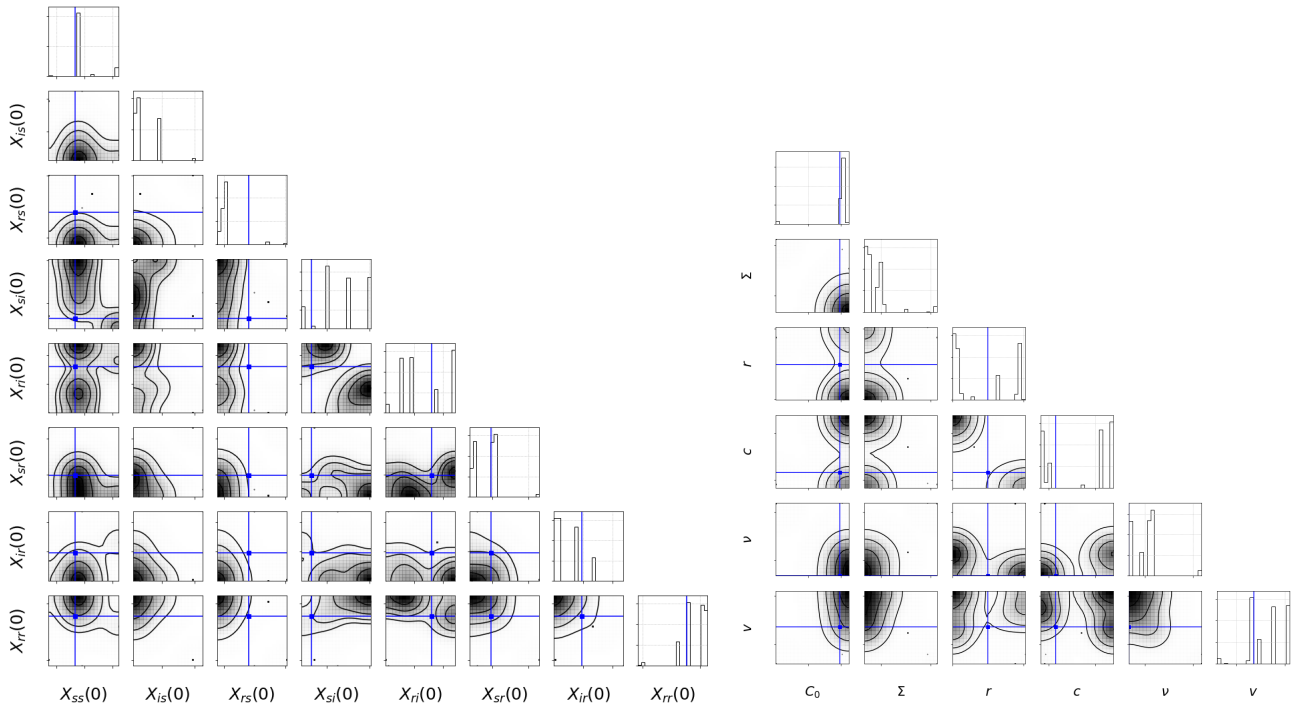

Figure 10: Analysis based on simulated data. Pairwise marginal contours for the initial conditions (left) and the auxiliary parameters (right). Blue lines represent the values of the simulation parameters for comparison.

August 2007 - July 2008

Table 7: Posterior summaries for the year 2007-08

Parameter	MAP	95% CIs	Parameter	MAP	95% CIs
β_1	44.6873	(42.3106, 64.1864)	X_{SS}	2285503	(2275957, 2284394)
β_2	74.3809	(68.8012, 77.8589)	X_{IS}	3834	(12, 4641)
σ_1	3.2271	(1.6241, 3.9189)	X_{RS}	34692	(35888, 51149)
σ_2	3.2649	(2.2319, 4.0325)	X_{SI}	1954	(403, 3944)
C_0	2.8743e-03	(8.3868e-03, 1.1844e-02)	X_{RI}	2187	(244, 7374)
Σ	3.3520e-07	(2.5413e-07, 4.9473e-07)	X_{SR}	26974	(14239, 28792)
r	0.06622	(0.057711, 0.07034)	X_{IR}	200	(41, 2493)
c	0.04461	(0.038592, 0.04900)	X_{RR}	144657	(141853, 151902)
ν	0.2130	(0.20471, 0.2579)			
υ	0.1478	(0.10015, 0.1312)			

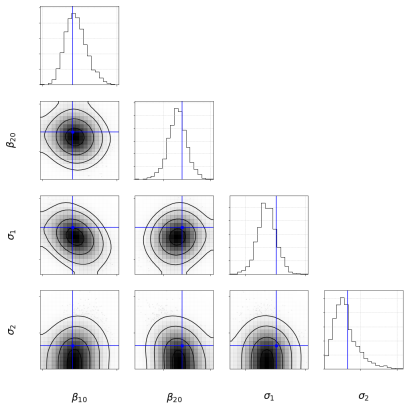

Figure 11: Analysis based on simulated data. Pairwise marginal contours for the parameters defining the stochastic kinetic model. Blue lines represent the values of the simulation parameters for comparison.

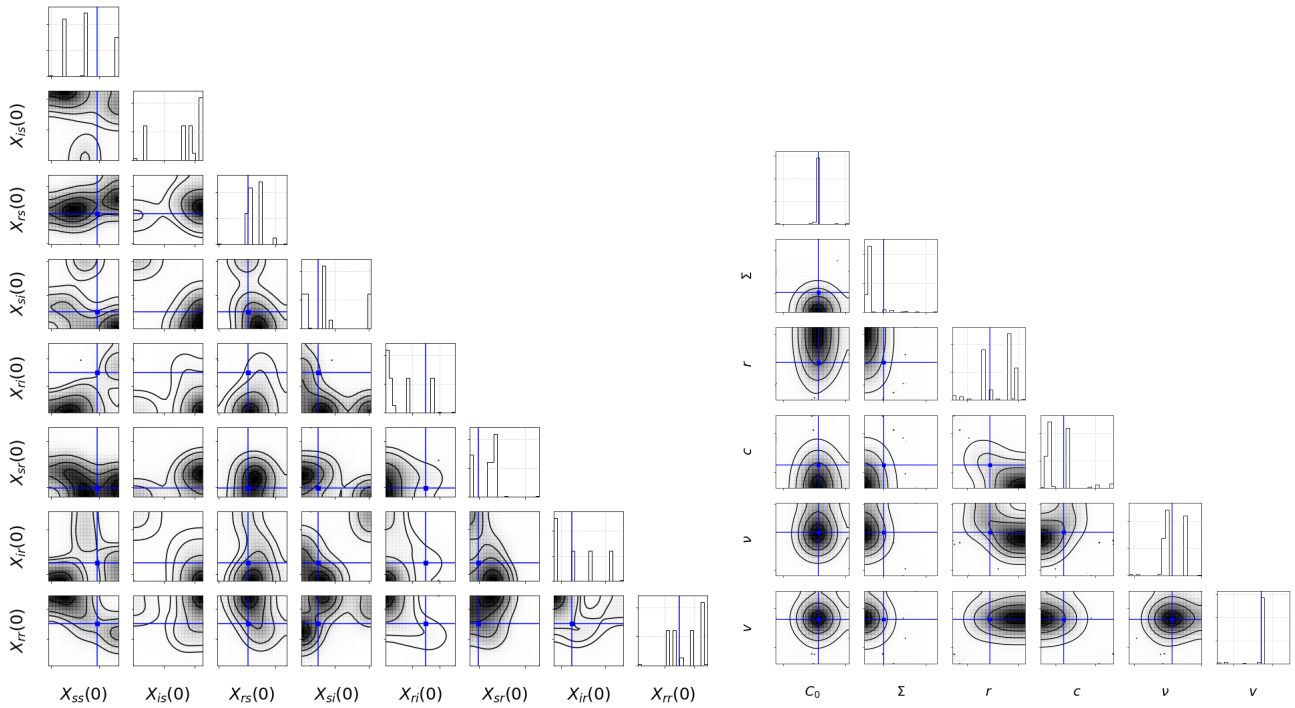

Figure 12: Analysis based on simulated data. Pairwise marginal contours for the initial conditions (left) and the auxiliary parameters (right). Blue lines represent the values of the simulation parameters for comparison.

August 2008 - July 2009

Table 8: Posterior summaries for the year 2008-09

Parameter	MAP	95% CIs	Parameter	MAP	95% CIs
β_1	22.69446	(47.4071, 72.6521)	X_{SS}	2218862	(2282264, 2352741)
β_2	65.7909	(61.7720, 69.6492)	X_{IS}	1530	(51, 4964)
σ_1	1.1189	(0.8197, 2.8442)	X_{RS}	171391	(21190 , 42842)
σ_2	0.7311	(1.7682, 12.3335)	X_{SI}	2758	(777, 7972)
C_0	5.6218e-02	(7.0720e-03, 1.2263e-02)	X_{RI}	4421	(291, 3925)
Σ	3.1020e-06	(2.0303e-06, 3.9120e-06)	X_{SR}	13593	(11606, 26648)
r	0.1042	(0.1077, 0.1609)	X_{IR}	3729	(8, 3539)
c	0.02627	(0.021435,0.02944)	X_{RR}	83717	(94793 , 147809)
ν	0.1673	(0.1984, 0.1994)			
v	0.2174	(0.08485, 0.09923)			

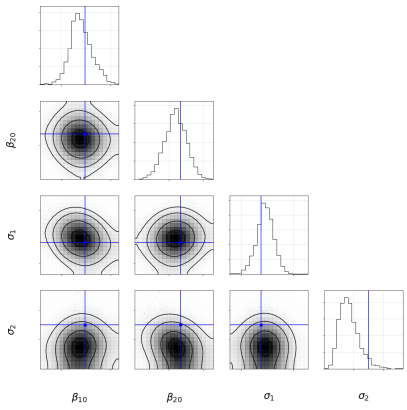

Figure 13: Analysis based on simulated data. Pairwise marginal contours for the parameters defining the stochastic kinetic model. Blue lines represent the values of the simulation parameters for comparison.

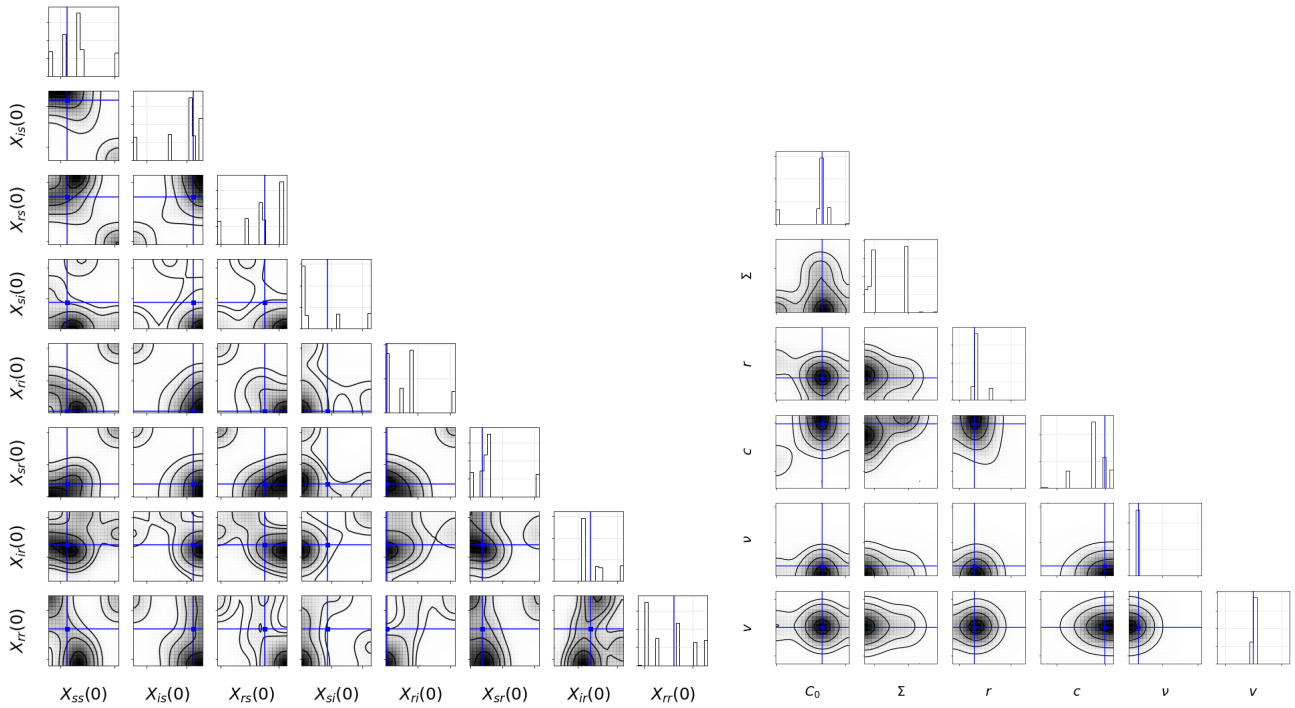

Figure 14: Analysis based on simulated data. Pairwise marginal contours for the initial conditions (left) and the auxiliary parameters (right). Blue lines represent the values of the simulation parameters for comparison.

References

Foreman-Mackey, D. (2016). "corner.py: Scatterplot Matrices in Python". *The Journal of Open Source Software*, 1(2).

Gillespie, D. T. (2007). "Stochastic Simulation of Chemical Kinetics". *Annu. Rev. Phys. Chem.*, 58:35–55.

Kamo, M. and Sasaki, A. (2002). "The Effect of Cross-Immunity and Seasonal Forcing in a Multi-Strain Epidemic Model". *Physica D: Nonlinear Phenomena*, 165(3):228–241.

Van Kampen, N. G. (1992). *"Stochastic Processes in Physics and Chemistry"*, volume 1. Elsevier.